ELSEVIER

Thermal camouflaging metamaterials

Run Hu [1], Wang Xi [1], Yida Liu [1], Kechao Tang [2], Jinlin Song [1], Xiaobing Luo [1,*], Junqiao Wu [2,*], Cheng-Wei Qiu [3,*]

[1] State Key Laboratory of Coal Combustion, School of Energy and Power Engineering, Huazhong University of Science and Technology, Wuhan 430074, China
[2] Department of Materials Science and Engineering, University of California, Berkeley, CA 94720, USA
[3] Department of Electrical and Computer Engineering, National University of Singapore, Singapore 117583, Singapore

Thermal camouflage technologies, which aim at blending the infrared (IR) signature of targets into the background to counter the IR detection, have witnessed increasing development. To achieve thermal camouflage, the rule of thumb is to balance the thermal radiation between the target and the background, and the corresponding conductive strategy is to tune the local temperature field while the radiative strategy is to tune the local emissivity. Following these two basic strategies, the thermal metamaterials and wavelength-selective emissivity engineering to achieve thermal camouflage are first introduced. Then the more advanced dynamic strategies are reviewed that can adapt to the varying environment under the external stimuli, like electricity, light, strain, chemical, wetting, temperature, etc. Particularly the phase-changing and bioinspired materials are presented and reviewed. Finally, critical considerations on the challenges and opportunities of next-generation thermal camouflage technologies are elaborated and four future directions are cast, including temperature-responsive emissivity engineering, soft materials, multispectral camouflage, and detection-feedback system. Overall, a detailed introduction to the working principle, the state-of-the-art progress, and the critical thinking on the future development on thermal camouflage technologies are presented.

Introduction

Over millions of years of natural evolution, many animals, like chameleon, squid, octopuses, cuttlefish, frog, etc., have developed the capability of camouflage that can blend themselves almost perfectly into the environment. Such kind of biological camouflage functions are not only exotic but also instructive for the camouflage technology development in multi-physical fields along with lots of applications like electromagnetic communication [1], military weapons [2,3], anti-counterfeiting [4], coating materials [5,6], deadening materials [7–9], temperature control [10–12], robot transformers [13–15], etc. Most of these natural animals with camouflage functionalities are in the visible spectra, while some are in the infrared (IR) spectra and the corresponding functionalities are called as thermal camouflage [16,17]. The IR camera interprets the detected radiative energy into electrical signals to display a pseudo temperature field, by which we can "see" the world at night like an owl. Since all objects emit thermal signals in a radiative way, the thermal signals, compared with the visible signals, are much easier to expose in the IR camera against the background temperature. Therefore, nowadays many modern military weapons are equipped with an IR camera to make the targets "visible" for detection and location. To confront the IR detection, the thermal camouflage technologies are demanded to conceal the targets in the IR camera by tuning the thermal radiation to be the same or similar with the background environment [18–21]. According to the working principle of an IR camera, i.e. Stefan-Boltzmann law $Q = \varepsilon\sigma T^4$ with ε the surface emissivity, σ the Stefan-Boltzmann's constant,

* Corresponding author.
E-mail addresses: Luo, X. (luoxb@hust.edu.cn), Wu, J. (wuj@berkeley.edu), Qiu, C.-W. (eleqc@nus.edu.sg).

1369-7021/© 2020 Elsevier Ltd. All rights reserved. https://doi.org/10.1016/j.mattod.2020.11.013

and T the absolute surface temperature, there are two basic strategies to achieve thermal camouflage: one is to change the local temperature T of the target, and the other is to tune the local surface emissivity ε of the target. Following these two strategies, the corresponding thermal camouflages are called as conductive and radiative thermal camouflage technologies respectively and lots of progress on thermal camouflage have been achieved in this decade [15,22,23].

To make the development history, working principle, and future trend of thermal camouflage clear for the readers, we would like to review the key milestones of thermal camouflage technologies here, which are shown in the timeline of thermal camouflaging metamaterials in Fig. 1. The hallmark technological transformation for thermal camouflage starts with conductive camouflage metamaterials that deals with temperature field, followed by the radiative camouflage that deals with the selective emissivity engineering. Due to the increasing demanding to confront with the detecting technologies for practical applications, multispectral camouflage and dynamic camouflage technologies are increasingly reported in recent years. The organization of this review can also be seen from Fig. 1. In Section 2, we review the conductive thermal camouflage in two subsections, i.e. tuning the in-plane and out-of-plane heat conduction for thermal camouflage, together with the brief introduction of the two basic design methods, i.e. transformation thermotics and scattering cancellation. Though some achievements have been made, the limitations of the conductive thermal camouflage will be discussed. In Section 3, we review the radiative thermal camouflage in terms of the emissivity-engineered and multispectral camouflage, which will be more practical and feasible in real applications. In Section 4, the dynamic thermal camouflage is reviewed through different strategies to achieve the dynamical tunability of the emissivity and thermal radiation, like the electricity-, light-, strain-, chemical-, wetting-, and phase-changing- tunable materials and bio-inspired materials. At last, the concluding remarks and perspectives are presented.

Conductive thermal camouflage

Conductive thermal camouflage aims at changing the surface temperature or to achieve thermal illusions near the target for thermal camouflage. It is well known that the governing equation of heat conduction is parabolic rather than hyperbolic, thus we cannot directly borrow the control approaches of wave optics to manipulate heat flow [24]. Heat conduction is diffusive and heat flux vector is path-dependent, and therefore achieving directional heat flow is challenging. Fortunately, with the advent of the artificial thermal metamaterials in last decade [25–27], their exotic and anisotropic characteristics of thermal properties endow the possibilities for the directional heat flow manipulation [28,29]. The so-called thermal metamaterials, as a large branch of the metamaterial family, are man-made anisotropic, inhomogeneous, and with-singularity structured materials, which possess the exotic thermal properties compared to the nature-existing homogeneous materials. Based on the thermal metamaterials, people have successively proposed and realize many novel thermal functionalities and devices, such as thermal cloaking [30–38], camouflage [39,40], illusion [41–45], concentrating [25,46,47], inverting [48], diode [49–50], lens [51], encoding [52], reflection [53], refraction [32], printing [54], etc. Among them, the thermal camouflaging metamaterial will be introduced here.

Design method

To achieve thermal functionalities and devices, there are two frequently-used design methods, which are introduced briefly

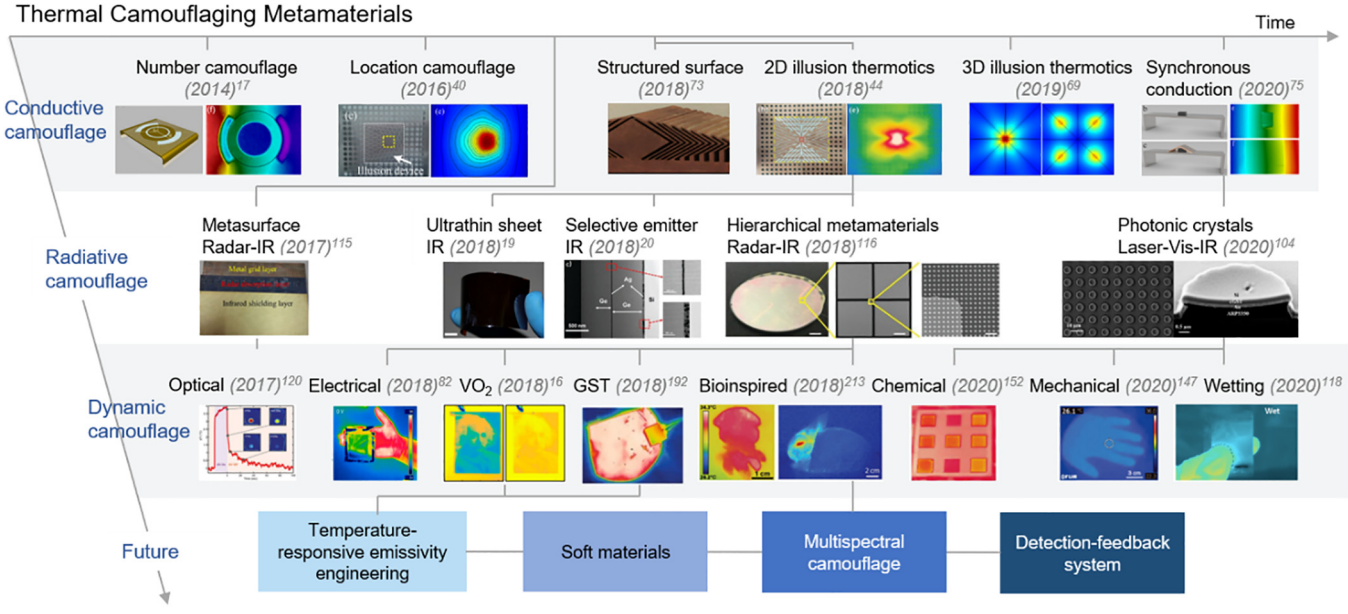

FIGURE 1

Timeline and roadmap for thermal camouflaging metamaterials from conductive, radiative, dynamic strategies, to the future directions.

as follows. Most of these thermal functionalities are designed by the transformation thermotics method [55–57]—the counterpart of the transformation optics theory—whose essence is the invariance of the governing equation in the coordinate transformation from one space to another. In heat conduction without heat sources, the governing equation $\rho c\frac{\partial T}{\partial t} = \nabla\cdot(\kappa\nabla T)$ is maintained as $\rho' c'\frac{\partial T'}{\partial t} = \nabla'\cdot(\kappa'\nabla' T')$, where ρ is the density, c is the specific heat, κ is the thermal conductivity, T is the temperature, and t is the time, respectively [58]. For steady state, the left hand of the governing equations vanishes. According to the transformation thermotics, the transformed thermal properties are $\kappa' = \frac{\mathbf{\Lambda}\kappa\mathbf{\Lambda}^{\mathrm{T}}}{\det(\mathbf{\Lambda})}$ and $\rho' c' = \frac{\rho c}{\det(\mathbf{\Lambda})}$ where $\mathbf{\Lambda} = \frac{\partial(x',y',z')}{\partial(x,y,z)}$ is the Jacobian matrix of the space/coordinate transformation. The transformed material thermal properties share the same functional forms as those in the transformed electromagnetics and optics, and that's why the transformation thermotics is named after the transformation optics. To achieve desired thermal functionalities, the real space (Ω') is usually stretched, compressed or rotated from the homogeneous virtual space (Ω). For instance, the seminal coordinate transformation for the two-dimensional (2D) thermal cloak is to compress a virtual cylinder with radius of b into an annular real cylinder with radii of a and b ($a < b$), leaving a null space with radius of a in the real space that corresponds to the singularity point in the homogeneous virtual space. Any objects sitting in the null space will be concealed from the exterior IR camera along the heat conduction plane, and will be free from the influence of exterior temperature change. The calculated thermal conductivity tensor for the 2D thermal cloak is $\kappa' = \mathrm{diag}\left(\frac{r'-a}{r'}, \frac{r'}{r'-a}\right)$, from which we can see that both the radial and tangential components of the transformed thermal conductivity are inhomogeneous, anisotropic and even with singularity at $r' = a$, and it is rather challenging to manufacture such kind of materials with nature-existing materials [50,59–61]. Schittny et al. fabricated a thermal cloak device by drilling a copper plate with holes, which were then filled with polydimethylsiloxane (PDMS) [62]. The distinct difference in thermal conductivities and the proper designed filling ratio made the effective thermal conductivity flexible for modulation. As shown in Fig. 2a, there are many concentric rings in the cloaking region, where the varying filling ratios make the local effective thermal conductivity close to the transformation thermotics design as much as possible. The transient IR experiments demonstrated that the central cylinder was cooler than its surroundings and the white isotherm lines on the downstream side the cloak tended to be vertical as if heat flows through a homogeneous plate.

Other than the transformation thermotics, the scattering cancellation method is also used to achieve thermal functionalities, which is originated for zero scattering cross section in optics, and has been extended for static magnetics, electrics and thermotics [17,63]. Though we seldom consider heat as thermal waves [64], this method can also be used to eliminate the distortion of isotherms in steady-state heat conduction field. When the core, shell and background thermal conductivities of a core–shell cloak structure are κ_1, κ_2, and κ_b respectively, the Laplace equation for steady-state heat conduction can be solved when setting the exterior heat flux to have no distortion and the core thermal conductivity $\kappa_1 = 0$. The required thermal conductivities of the shell are $\kappa_2 = \frac{b^2+a^2}{b^2-a^2}\kappa_b$ in cylindrical coordinate and $\kappa_2 = \frac{2b^3+a^3}{2\left(b^3-a^3\right)}\kappa_b$ in spherical coordinate. This method is relatively simple but only applicable for exterior homogenous temperature

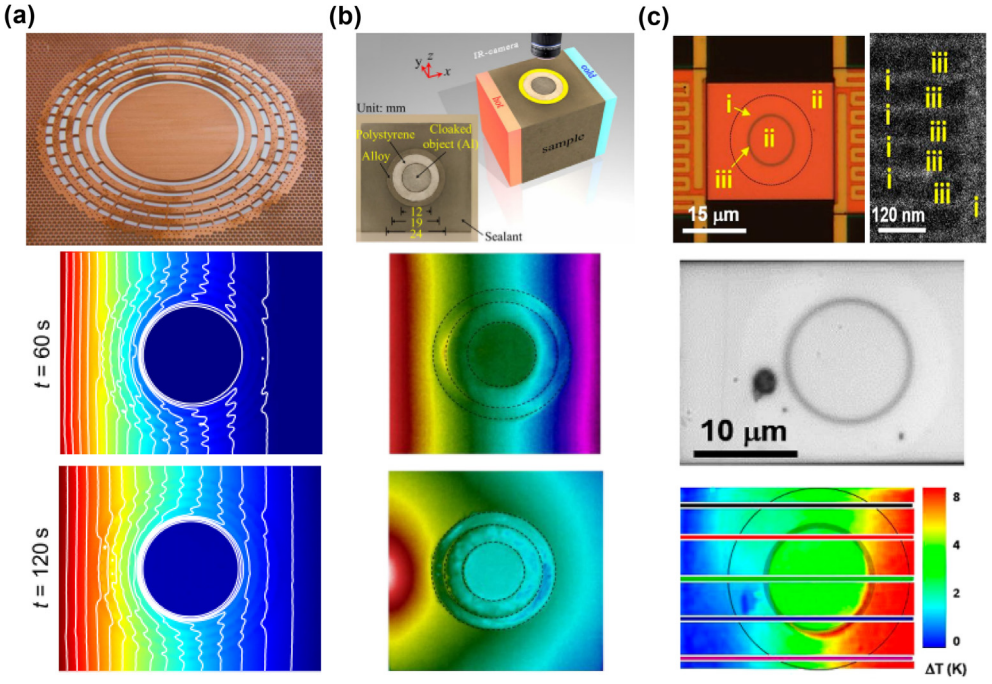

FIGURE 2

Experimental demonstration of thermal cloaking by (a) transformation thermotics [62], Copyright 2013, American Physical Society. (b) Scattering cancellation [65], Copyright 2014, American Physical Society. (c) Microscale helium ion irradiation [70]. Copyright 2019, American Chemical Society.

gradient. From the formula, we can see that the calculated thermal conductivity is homogeneous and isotropic, which can be fabricated with nature-existing materials. This is the advantage over the transformation thermotics, but due the compromise controllability and tunability, the performances of the thermal functionalities are limited. Han et al. followed this strategy and designed a bilayer thermal cloak with demonstration of thermal cloak experimentally [65]. As shown in Fig. 2b, the 2D bilayer cloak was made by expanded polystyrene and 625 alloy immersed in the host background materials of sealant. The radii of the bilayer cloak were designed according to above formula. The experimental IR images for the uniform and non-uniform temperature fields validated that the core cylinder was cloaked with uniform temperature. Such good demonstration reveals that regular bulk materials can also be used to design and fabricate thermal cloaking devices for practical engineering applications. Besides, some thermal cloaks or illusion devices are designed by topology optimization method, which provide another route for practical implementation via the existing isotropic materials [66,67].

Besides such macroscale demonstrations, the thermal cloaking effect are also explored in the microscale to tune heat flow with potential applications in thermal management for microelectronics and nanoelectronics [68,69]. Choe et al. developed an ion-write micro-thermotics (IWMT) device, on which they tuned the local thermal conductivity of silicon membrane from the crystalline value to the amorphous value by modulating the dose of helium ion beam irradiation to achieve the microscale thermal cloaking demonstration [70]. They designed a bilayer thermal cloak on the IWMT device, as shown in Fig. 2c, and adopted the noncontact thermo-reflectance imaging (TRI) technique to map the microscale temperature field. It is seen that the region (ii) temperature is nearly uniform, as most heat was routed by the pristine region (i) and blocked by the heavily irradiated region (iii). The essence of their IWMT device is the two-dimensional phonon engineering, which is a significant progress for both phonon engineering and thermal metamaterials, and may trigger more microscale thermal functionalities beyond thermal cloaking.

In-plane heat conduction

Among the thermal functionalities, thermal cloaking is to change the thermal signature of an arbitrary object into nothing, and thermal camouflage is to make the signature of one object invisible from the background. Therefore, in broad sense, these functionalities can be unified as thermal camouflage. After the advent of thermal metamaterials, the first thermal camouflage device was reported by Han et al. in 2014 [17]. They transformed the thermal scattering signature of a cylinder into multiple isolated expected objects. As shown in Fig. 3a, with their thermal camouflage device, the "man" is camouflaged into two "women" from the same thermal signature. To design such a camouflage device, the scattering cancellation method is used by two steps. They eliminated the scattering of the original object through the designed bilayer cloak, and then generated the desired scattering signature by placing proper objects. The experimental samples were manufactured by drilling holes into a copper plate and the holes were filled with PDMS, as shown in Fig. 3a. The measured temperature fields with comparative case are shown in Fig. 3a and we can see clearly that the exterior temperature fields are almost the same though the two experimental samples are totally different. Through this device, the inner copper cylinder is thermally camouflage. Later, the illusion thermodynamics, derived from the transformation thermotics, is proposed to define a thermal reshaper that can reshape an arbitrary object into another with arbitrary cross section in two steps. More interestingly, the reshaper can unify the cloak, concentrator, amplifier, and shrinker, depending on the desired functionalities [71]. In 2016, Hou et al. designed a planar camouflage device to move the heat source from one position to another while the temperature profile outside the device appears to be produced by the moved virtual heat source [40]. To facilitate the experimental fabrication, linear coordinate transformation is used, which can ensure the homogeneity of thermal conductivity in the transformed space. The comparative experimental samples and measured temperature fields are shown in Fig. 3b, including a heater without the device on the right (Case 1), a heater with the device on the right (Case 2), and a heater without the device on the left (Case 3). Although the heat source is the same location in Cases 1 and 2, the temperature fields outside the device in Case 2 is different from that in Case 1 and the same as that in Case 3 instead. So from the outside temperature field in Case 2, we may perceive that the heat source is located at the left (Case 3) rather than the right (Case 1). In this way, the location of the heat source is camouflaged. These conductive thermal camouflages only maintain the outside temperature field. However, from the whole IR picture, we can easily locate the cylinder copper in Fig. 3a and the heat source in Fig. 3b. To solve this problem, Hu et al. in 2018 added the splitting function into the previous thermal camouflage devices, and proposed the concept the illusion thermotics unambiguously as a general design rule for conductive thermal camouflage device [44]. As shown in Fig. 3c, besides maintaining the same outside temperature curve, multiple local temperature peaks are created with the real heat source among them. In this "interior splitting + exterior illusion" way, not only from the outside temperature field but also from the inner temperature field, we cannot easily to locate the heat source. Experiments and simulations are conducted to validate the idea successfully. Further Hu and colleges extended the illusion thermotics to 3D version to achieve the separated thermal illusions vividly [72]. Though only one heat source was located at the bottom surface, four thermal illusions were observed from the top surface, thus the heat source was thermally camouflaged.

Out-of-plane heat conduction

The conductive thermal camouflages tune the in-plane heat conduction, and we also can tune the out-of-plane heat conduction to achieve camouflage [73]. Considering a camouflage device that covers an object against a background plate, if the surface temperature of the camouflage device equal to the background plate point by point in the projected domain, the covered object will be concealed instead, which looks as if the object is nonexistent. To achieve such a camouflage device, in Fig. 4a, Li et al. used two consecutive transformation thermotics to design a conductive structure without a priori knowledge of the back-

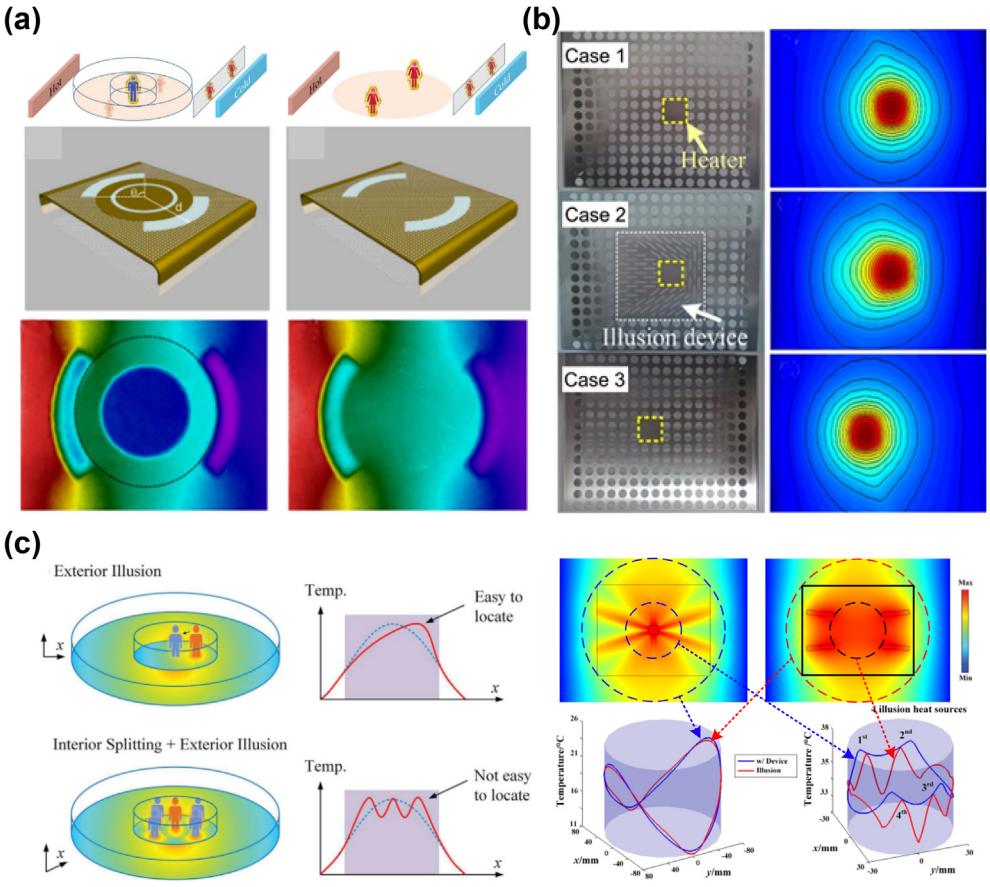

FIGURE 3

In-plane conductive metamaterials for thermal camouflage. (a) A camouflage device enabling an object to possess arbitrary wing-ghosts off its original position and produce equivalent outside temperature profile [17]. Copyright 2014, Wiley-Blackwell. (b) Photographs of a planar illusion device and corresponding measured temperature fields, comparatively demonstrating the delocalization of a heat source with same temperature profiles outside the device [40]. Copyright 2016, American Institute of Physics. (c) Schematic of heat source-targeted illusion thermotics and comparative temperature fields to show the "inner splitting + exterior illusion" function for practical thermal camouflage, which not only maintain the outside thermal camouflage but also mislead the number, location, shape, and rotation information of the heat source [44]. Copyright 2018, Wiley-Blackwell.

ground temperature [6]. The object temperature below the camouflage device is replaced with a temperature profile that is identically mapped from the background. The key point is that heat is conducted from the background to the camouflage device point by point vertically, thus the temperature profile on the background is shifted to achieve thermal camouflage. The experimental results validate the idea perfectly. As shown in Fig. 4a, the temperature of the object with the camouflage device is identical to the background plate without an object. They further extended the 2D metamaterials-based thermal camouflage device into a 3D version with enhanced detection-angle compatibility [74]. Besides the vertical heat conduction, there is another route to achieve such temperature shifting. As shown in Fig. 4b, to camouflage the target, Zhang et al. maintain the surface temperature of the device (T_d) and background plate (T_b) as the same from point to point in the projected area of the camouflage device, i.e. $T_d \equiv T_b$ with $x \in [a, b]$ in Fig. 4b, so that the observed the IR images will be the same as that of the pure background plate [75]. After rigorous mathematical deduction, the design rule to achieve a camouflage device is $\alpha_d = \left[1 + \tan^2\theta\right]\alpha_b$, where α_d and α_b are the diffusion coefficients of the device and the background plate, and θ is the tilt angle of the camouflage device. Following this design rule, they designed a copper device on an aluminum background plate. Through both simulations and experiments, the temperature curves on the device (T_{d1} and T_{d2}) overlap with those points vertically on the background (T_{b1} and T_{b2}), validating the perfect thermal camouflage performance dynamically. The experiment shows that the device can well camouflage the target. Both simulations and experiments validate the feasibility of thermal camouflage base on the tuning of out-of-plane heat conduction.

Radiative thermal camouflage

Another route to achieve thermal camouflage is to tune the surface emissivity to make the detected thermal radiation energy from the target object approximate to that of the background [12,76–78], and consequently the target will be concealed in an IR detector. Usually, the background temperature is below the target temperature, and thus reducing the surface emissivity is a typical and effective way to decrease the thermal radiation energy. For instance, people choose metal or low emissivity coatings or films to suppress the thermal radiation [79,80]. However,

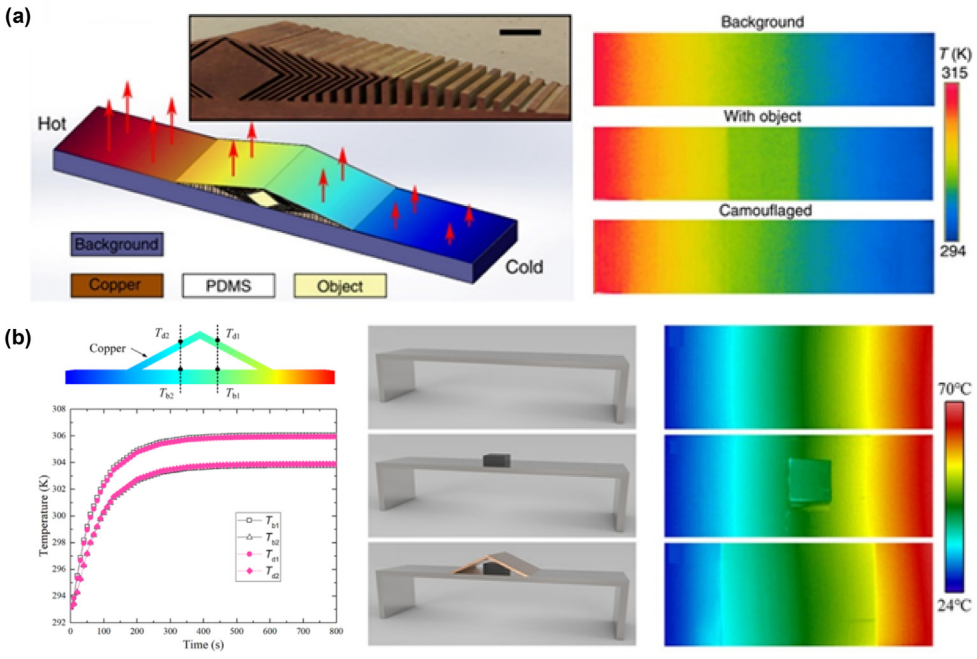

FIGURE 4

Out-of-plane conductive metamaterials for thermal camouflage. (a) Photograph and schematic of the copper device, and the experimental validation of the thermal camouflage performance [6]. Copyright 2018, Nature Publishing Group. (b) Simulations of the synchronous heat conduction along the copper device and the background plate, and the experimental setup and demonstration of thermal camouflage performance [75]. Copyright 2020, IOP Publishing Ltd.

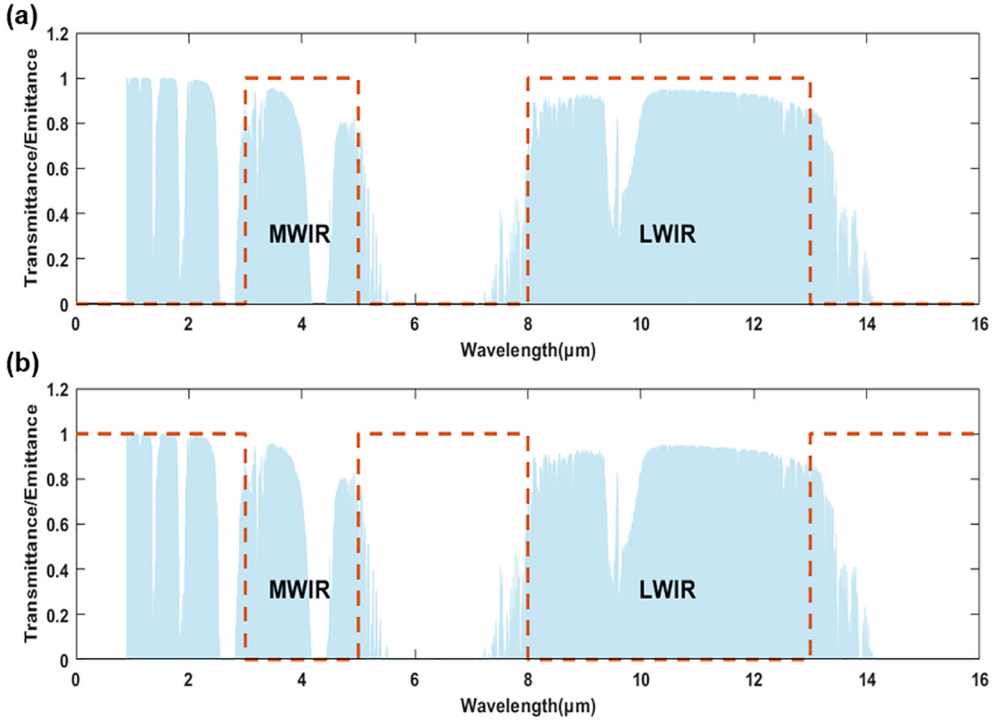

FIGURE 5

Ideal emissivity spectrum for thermal camouflage at (a) high and (b) low background temperatures. Shadow regions denote the atmosphere transmittance.

this will reduce the radiative heat dissipation and will cause temperature rise in return. The Stefan-Boltzmann law tells us that thermal radiation power is proportional to the fourth power of temperature (T^4). Therefore, even a small temperature rise may enhance the thermal radiation power and weaken the thermal camouflage performance significantly. On the other hand, low emissivity treatments result in high reflection, which will be detected from the reflected signals and thus destroying the camouflage performance [81,82]. To overcome such paradox, wavelength-selective emissivity engineering is required to achieve practical thermal camouflage [83–85].

Ideal emissivity spectrum for thermal camouflage

The atmosphere transmittance curve is shown by the shadow region in Fig. 5, from which we can see that there are two wavelength ranges with high transmittance, i.e. mid-wavelength IR (MWIR) range (3 ~ 5 μm) and long-wavelength IR (LWIR) range (8 ~ 14 μm). These two ranges are called as atmosphere windows. Due to the high transmittance, thermal radiation within MWIR and LWIR ranges will be directly emitted, and most IR detectors also work in this two frequency ranges to enhance the general application scenarios. As discussed above, the purpose of thermal camouflage is to balance the thermal radiation energy of the targets and the background, thus it is perceived that the ideal emissivity spectrum depends on the background temperature. When the background temperature is low, the detected thermal radiation energy should be reduced to blend into the background, so as shown in Fig. 5b, the emissivity inside the two atmosphere windows should be low, depending on the background temperature, while the emissivity outside the MWIR and LWIR ranges remains as high as possible to further cool the surface for better radiative heat dissipation. However, when the background temperature is high, as shown in Fig. 5a, the scenario is just opposite that the emissivity should be high at MWIR and LWIR ranges to enhance the thermal radiation of the target to match with that of the background, while the emissivity outside MWIR and LWIR ranges remains low to reduce the heat dissipation. From Fig. 5, it is seen that the ideal emissivity spectrum changes with the background temperature, but the rule of thumb is to maintain the equivalent thermal radiation energy between the targets and the background in the working wavelength ranges of the IR detectors. In essence, thermal camouflage is a special thermal management problem. For this end, such wavelength-selective emissivity spectrum can be achieved for thermal camouflage by modulating materials, surface nanostructure, treatment, etc [84,86–93].

Emissivity-engineered thermal camouflage

Following the emissivity engineering roadmap, people have proposed different strategies for thermal camouflage. Moghimi et al. fabricated silicon nanowires (SiNWs) and silver nanoparticles (AgNPs) onto a host flexible polyimide sheet to achieve a wideband thermal camouflage, as shown in Fig. 6a [19]. SiNWs serve as an excellent antireflection coating to minimize the

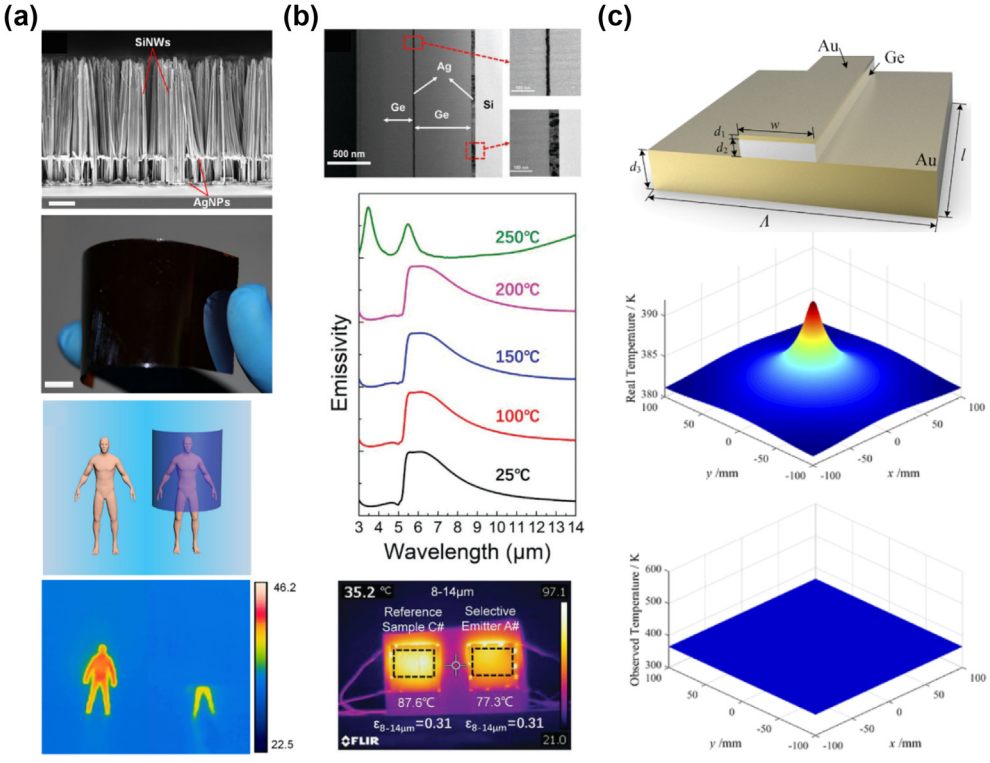

FIGURE 6

Emissivity-engineered materials for thermal camouflage. (a) SEM image for a forest of dense SiNWs 11.79 μm long with diameters varying from 50 to 500 nm, photograph of a camouflage sheet with a 120 μm thick polyimide layer along with embedded SiNWs and AgNPs, and the comparative thermal camouflage performance [19]. Copyright 2018, Wiley-VCH Verlag. (b) HRTEM image of the Ag/Ge multiplayer film, measured emissivity spectra from 25 to 250 °C, and the IR image of selective emitter (A#) and a reference sample (C#) through the IR camera with the working frequency range of 8 ~ 14 μm [20]. Copyright 2018, John Wiley & Sons Inc. (c) Schematic for the unit cell MIM structure, the real temperature field and the corresponding observed temperature field [98]. Copyright 2018, Optical Society of America.

reflection from the surfaces. AgNPs are distributed between the SiNWs to absorb the incident EM waves as much as 95%, which is turned into heat and then dissipated by the air channels between the SiNWs without temperature rise. As such, the microscale emitter array can remain low temperature to against the disguise and deception. The IR experiment on a human model in Fig. 6a verifies that the model without the camouflage sheet is vividly detectable while the top half of the model covered by the sheet is invisible, validating the thermal camouflage performance.

Note that the thermal camouflage achieved in their flexible sheet is due to the relatively low emissivity in a broad spectrum without wavelength selectivity, which only works at the cold background temperature. For better thermal camouflage performance, the wavelength-selective spectrum is demanded. Peng et al. designed a wavelength-selective emitter based on silver/germanium (Ag/Ge) multilayer film to achieve thermal camouflage [20]. The thermal emission can be tuned by the layer thickness of the Ag/Ge multilayer based on impedance matching [93]. After parameter optimization, the cross-sectional high-resolution transmission electron microscope (HRTEM) image is shown in Fig. 6b, whose measured emissivity is low at the two atmosphere windows for thermal camouflage and is high in between for radiative cooling to further decrease the temperature. It is seen that the fabricated emitter retained the selective thermal radiation characteristics from room temperature up to 200 °C. The thermal camouflage performance is characterized by comparing with a low-emissivity material reference sample of the same size. As shown in Fig. 6b, the fabricated Ag/Ge multilayer selective emitter has lower temperature than the reference one due to the radiative cooling effect in 5–8 μm. Zhu et al. combined a silica aerogel and a Ge/ZnS multilayer for high-temperature thermal camouflage with efficient radiative cooling capability [94]. The silica aerogel is used for thermal insulation to suppress the thermal radiation partially from the high-temperature target. The emissivity at 8–14 μm is low for thermal camouflage, while at $5 \sim 8$ μm is high for radiative cooling. Experiments demonstrated that the object placed indoor/outdoor at temperature of 873 K and 623 K exhibit good thermal camouflage effect at 310 K and 248 K, respectively. Song et al. designed the metasurface with metal/insulator/metal (MIM) [95–97] structures to tune the surface emissivity spectrum [98]. The surface emissivity is strongly dependent on the MIM structure, and the authors firstly set up a database about the MIM structure and the emissivity spectrum. Then by screening the whole plate with proper structure design, the same thermal emission energy from each unit cell can be achieved although the temperatures of each unit cell structure are not consistent. Due to the heat source, the real temperature field was not uniform, but the observed temperature field was uniform and as shown in Fig. 6c, the heat source was thermally camouflaged. They further extended this strategy for the liquid crystal-based MIM structure for dynamic thermal camouflage by concealing the real heat source even though it was moving [99].

Multispectral camouflage

To confront with camouflage technologies, modern detecting technologies have been developing faster with multi-band detecting technologies for better target identification, like in the visible, IR, laser, and radar [100,101]. Once the single-band signals are camouflaged, the target may still be detected in other bands, thus the multispectral detecting technologies garner increasing attentions. To cope with the multispectral detection, the multispectral camouflage materials and structures, therefore, are strongly demanded to hide targets over a broad wavelength, and the multispectral camouflage materials and structures [102–107] are strongly demanded to hide targets under complex situations, especially for radar and IR camouflage technologies since radar and IR camera are the most widely used detection measures [108–110]. Except for the ideal emissivity spectrum, high absorptivity and low reflection are required at radar working wavelength (say 10.6 μm CO_2 laser radar) [111]. It is rather challenging to achieve such multispectral camouflage since the requirements on the emissivity spectrum, sometimes, are competing intrinsically [111]. In recent years, though the radar camouflage has made some progress in microwave band based on the metamaterial absorbers [112–114], the compatible camouflage is relatively rarely reported. Zhong et al. utilized the concept of multifunctional metasurface stacks to achieve a radar-IR camouflage compatible three-layer composite structure, including an IR shielding layer (IRSL), a radar absorption layer, and a metal grid layer, as shown in Fig. 7a [115]. The radar absorption layer is made by a double square loop (DSL) array to achieve the perfect metamaterial absorber from microwave to optical band. The simulated and measured absorptivity for transverse electric (TE) polarizations in $2 \sim 10$ GHz is shown in Fig. 7a, from which we can see that 90% bandwidth of the radar absorption is from 3 to 8 GHz. The transmission of the IRSL and substrate is measured from 1.7 to 20 μm, and the transmission peaks of the IRSL are only 1.8% in the range of $3.5 \sim 6.5$ μm. IR measurement was also conducted to show the thermal camouflage performance with comparison to a blackbody reference sample. Due to the low IR emissivity of the IRSL, the IRSL shows lower temperature than the reference sample, though they are at the same temperature.

Note that although they have achieved the radar-IR camouflage compatibly, the thermal camouflage is based on the low emissivity without wavelength selectivity. This may lead to thermal instability for some materials and structures since both the absorbed microwave energy and heat generation may create a significant thermal load and lead to the deterioration of thermal camouflage. To overcome this, Kim and coworkers proposed a hierarchical metamaterials (HMMs) to achieve multispectral camouflage with wavelength selectivity [116]. The HMM structure consists of an IR-selective emitter (ISE) on top of a microwave-selective absorber (MSA). The ISE achieves the ideal emissivity spectrum as Fig. 5b that the emissivity is low at MWIR and LWIR wavelengths, and is high elsewhere. Due to the significant change in the working wavelength, the challenge for the HMMs is the fabrication of different size structures from several millimeters to micrometers. Fig. 7b show the scanning electron microscope (SEM) images of the ISE, MSA and HMM. The measured emissivity over the IR wavelengths and the absorptance over the microwave wavelengths are shown in Fig. 7b. It is seen clearly that the HMMs possess the selective emissivity for thermal camouflage as the ISE and broad absorptance for radar camouflage as the MSA. The IR and radar cross section (RCS)

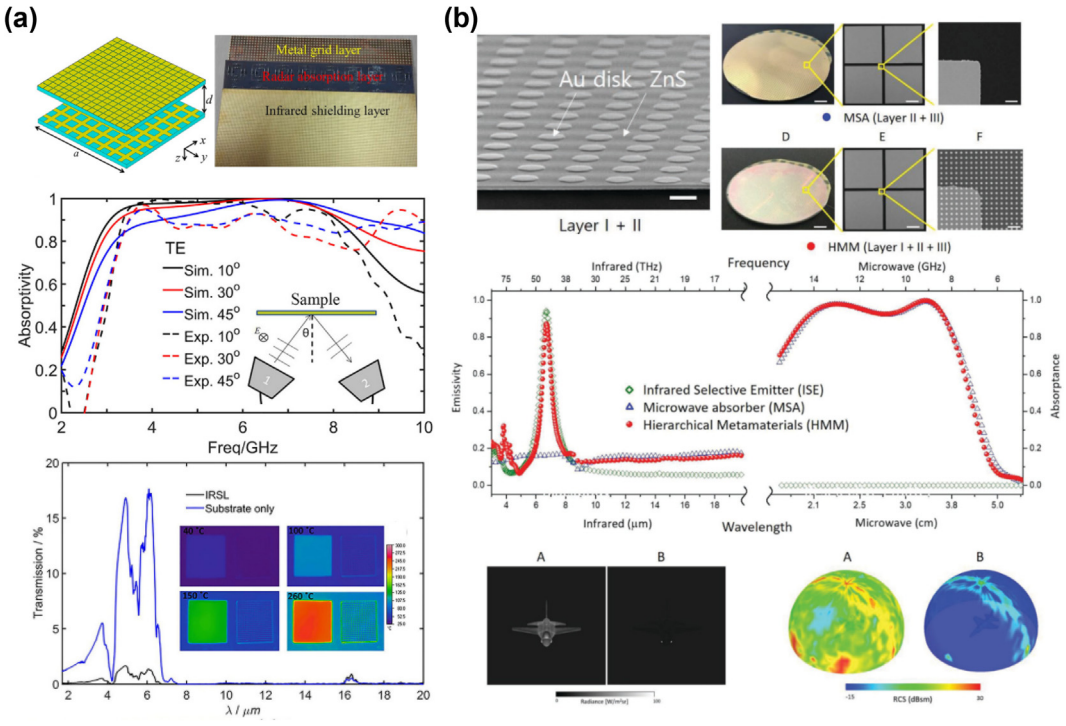

FIGURE 7

Multispectral camouflage materials. (a) Schematic and photograph of the radar-IR bifunctional device, simulated and measured absorptivity for TE polarization at different incident angles, and the measured transmission of the device and substrate with insetting the IR images of a blackbody (left) and the device (right) at different temperatures [115]. Copyright 2017, American Institute of Physics. (b) SEM images for the IR selective emitter (ISE), microwave selective absorber (MSA), and hierarchical metamaterials (HMM), measured multispectral emissivity over the IR spectrum and absorptance over the microwave spectrum, and simulated IR and microwave camouflage performances [116]. Copyright 2019, Wiley-VCH Verlag.

simulations reveal that the HMMs can reduce the signature of the target in the IR and microwave ranges by up to 95% and 99%, respectively, thus achieving the multispectral camouflage.

Dynamic thermal camouflage

The aforementioned emissivity engineering, achieved by different materials and structures, is usually fixed, such that the targets can only be thermally camouflaged at a fixed background temperature. While in real applications, the targets may be movable or the background temperature may change; once such situation happens, the static thermal camouflage performance will be deteriorated significantly and the camouflaged targets will be detected due to the inconsistency of the IR signatures of the targets against the background. Therefore, the dynamic thermal camouflage, compared to the static one, is much practical and promising in the future military applications. For this end, the desired dynamic thermal camouflage requires an adaptive material that can be actuated under the external stimuli, like electricity, light, temperature, wetting, mechanics, vapor, etc [3,15,81,117–120]. To date, several strategies have been implemented to engineer the thermal emissivity, and some of them have been applied to achieve the dynamic thermal camouflage functionality.

Electrical modulation

It has been long to know that electricity can be used to tune the thermal emission of materials, based on which Thomas Edison invented the incandescent light bulb in 1878. As electricity is more flexible to modulate, electrical stimulus has been used to tune the thermal emission for different applications including camouflage [121–125]. Inoue et al. demonstrated the dynamic control of surface emissivity in an n-type GaAs/$Al_{0.3}Ga_{0.7}As$ quantum wells (QWs) [117]. The n-type QWs induce an intersubband transition between two quantized energy levels in the conduction band, which yields narrowband absorption at the transition wavelength. The key characteristics of the QW structure is the magnitude of the intersubband absorption can be externally controlled by the external applied voltage. The electrically modulated thermal emission is observed by an IR camera at 100 °C with and without an applied reverse bias of 10 V, as shown in Fig. 8a, from which we can see that the thermal radiation is modulated by the voltage bias. When the QW is biased, the thermal emission is suppressed significantly, which may be applicable for thermal camouflage. More importantly, this work shows the feasible electrical modulation of surface emissivity and thermal radiation at a short timescale, much faster than typical thermal cycling times.

Other than QWs, the 2D materials like graphene, due to their good plasmonic resonance in the IR and terahertz ranges, shows strong EM response modulation by the external electrical stimulus [126–130]. The linear band structure and 2D nature enable the support of plasmonic modes with a unique dispersion relation, making it feasible for strong absorption control. The intensity and frequency of these plasmonic modes are carrier density

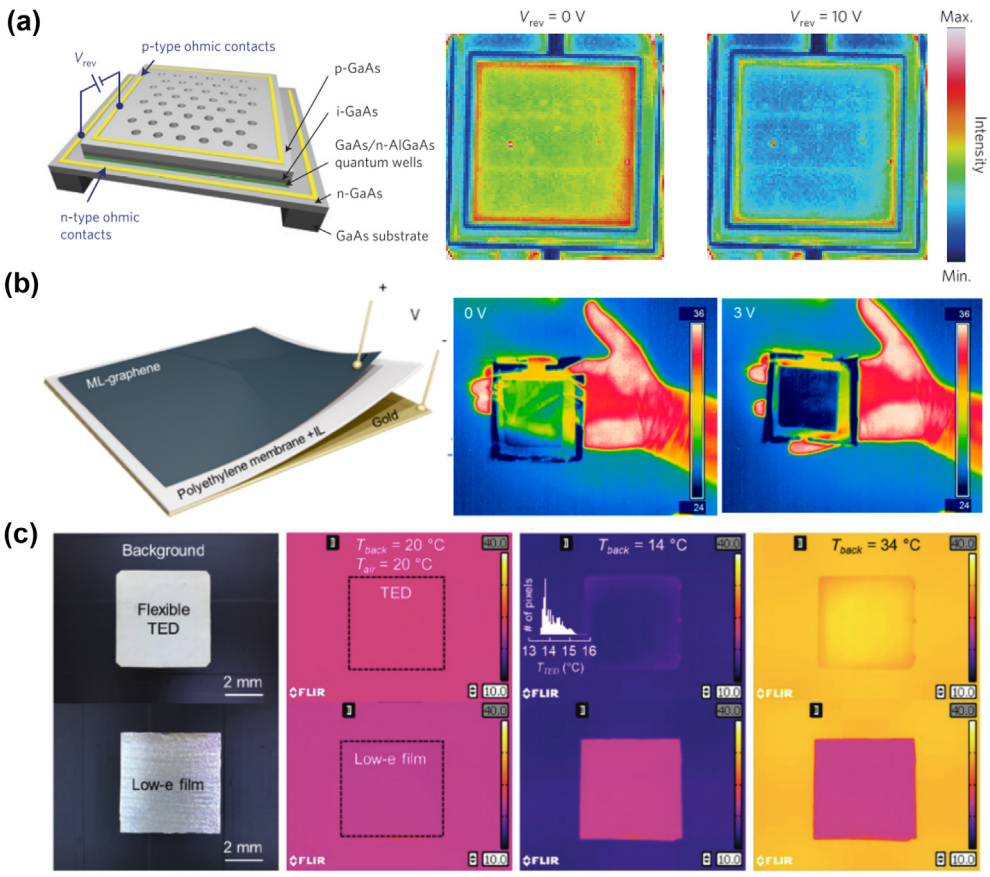

FIGURE 8

Electricity-modulated materials for thermal camouflage. (a) Schematic of the quantum well device, and the IR images of the device at 100 °C with and without the reverse bias [117]. Copyright 2014, Nature Publishing Group. (b) Schematic of the graphene-based adaptive thermal camouflage, and the IR images of the devices on hand under the voltage of 0 and 3 V [82]. Copyright 2018, American Chemical Society. (c) Dynamic thermal camouflage performance comparison between flexible TED and low-e film at difference background temperatures [141]. Copyright 2019, Wiley.

dependent, thus by tuning the density of the high-mobility free carriers, the EM radiation of graphene can be controlled in a broad spectrum from visible, IR, to microwave frequencies [82,131–135]. Salihoglu et al. developed adaptive thermal camouflage structure by multilayer graphene framework with ionic liquid inside [82]. When a voltage bias is applied, the ionic liquid is driven to dope the graphene layers. As a result, the local charge density and the Fermi level increases to suppress the IR absorption and emissivity. The vivid experiments in Fig. 8b validate that at 3 V bias, the structure's emissivity is suppressed significantly, and the detected energy approximates to that of the background to camouflage a human hand. While without a voltage bias, the human hand can be seen from the IR image due to the higher temperature of the hand and the original same emissivity of the graphene. It is worth noting that the emissivity of the structure can be switched for many times with a rather short switching time (<1 s). Moreover, the graphene-based structure is thin, light, and flexible, thus it is easy to implement for practical adaptive thermal camouflage. Similar to graphene, other 2D materials whose thermal radiation energy can be tuned by electricity can also be applied for thermal camouflage, and the only concern is that whether the adjustable extent of thermal radiation energy is large enough with cognizable temperature difference in the IR detectors. This is an interesting question that is worth of further exploring in the near future.

The above strategies are based on tuning the surface emissivity, but electrical modulation can also be used to achieve desired surface temperature by electrical heating or cooling through the thermoelectric devices (TEDs) [136–140]. More importantly, the fast temperature modulation through TEDs can be used for dynamic thermal camouflage, showing much superiority over the low-emissivity (low-e) coatings or films. Low-e coatings or films only applicable for low-temperature environment, where suppressing the thermal radiation of the targets is required to achieve the equivalent radiation level with the background. But when the background temperature is high, such low-e strategies will, rather than helping on achieving thermal camouflage, expose the targets due to the enhanced radiation distinction with the background. For this end, Hong et al. fabricated flexible TED for active and wearable thermal camouflage applications [141]. The comparative experiments in Fig. 8c show that the flexible TED can achieve better thermal camouflage at different background temperatures dynamically, while the low-e film can only achieve thermal camouflage at some certain background temperature. They further demonstrated the dynamic thermal camouflage performance on human arms within a wide range of background temperature.

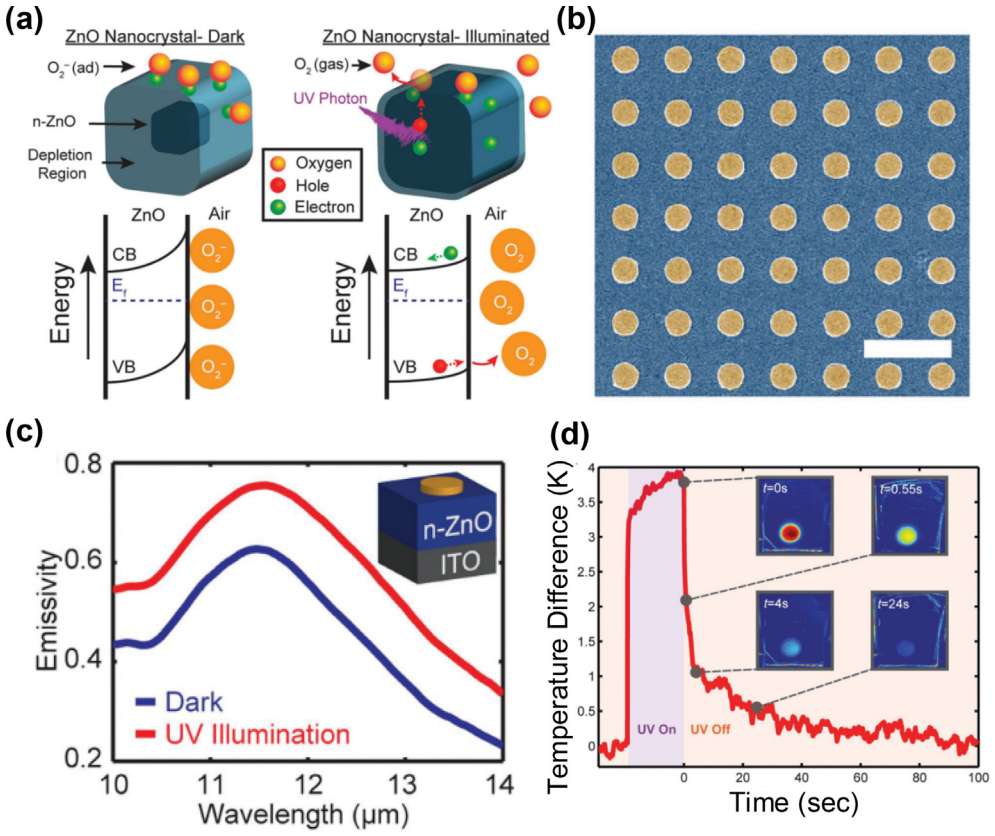

FIGURE 9

Light-modulated materials for thermal camouflage. (a) Schematic of ZnO nanocrystal under dark and illuminated condition with corresponding energy diagrams. (b) Experimental sample. (c) Measured spectral emissivity of the metamaterial before and after UV illumination. (d) Temporal response of metamaterial with the change of illuminated spot temperature [120]. Copyright 2017, Wiley.

Optical modulation

In contrast, the optically modulated emissivity engineering is scarcely reported. Coppens and Valentine demonstrated the spatiotemporal emissivity control on a large-area IR metamaterial by modulating with ultraviolet (UV) light [120]. As shown in Fig. 9a, in dark condition, oxygen molecules absorb to zinc oxide (ZnO) nano-crystallite boundaries and trap free electrons, where the built-in potential cause the separation of photo-generated electrons and holes. When illuminated, the adsorption and desorption process increase the free carrier concentration, leading to the increase of surface emissivity. Note that this process is reversible, which means that once removing the UV light, the emissivity returns to its original state. The photocarrier doped ZnO is chosen here because it has a long photocarrier lifetime, benefiting for the subsequent modulation. The fabricated ZnO metamaterial is shown in Fig. 9b, and the resulting emissivity increases by 0.16 in peak and 0.12 in total. The IR experiment in Fig. 9c and 9d show that UV can play the role of a special switch for the emissivity in modulating the surface temperature. Note that the recovery time is that fast, but it is not detrimental for thermal camouflage, in which the emissivity should be controlled at approximate change speed of the background temperature. Note that the ZnO nanocrystal here is just an example for the demonstration of emissivity engineering based on optical modulation, and other semiconductors are also worth of future exploring to improve the modulation performance in terms of the adjustable range and dynamic properties for potential thermal camouflage applications. Besides UV light, Xiao et al. demonstrated that the thermal emission can be modulated from heated semiconductors by a visible pulsed laser [142]. When the pump is turned on, the increased free carriers enhance the emissivity due to the strong absorption of the incident above-gap photon energies; when the pump is turned off, the free carriers recombine and the emissivity decreases. Note that such emissivity modulation is based on the free carrier, and the response time can be as short as the scale of the free carrier lifetime, like a few nanoseconds for GaAs and a few microseconds for Si. Therefore, such optical modulation can be used for fast tuning for thermal emissivity, which shows potential for adaptive thermal camouflage.

Strain modulation

Mechanical strain could change the surface appearance and can also be used to modulate the IR characteristics with potential for thermal camouflage. Liu and Padilla proposed to dynamically tune the surface emissivity based on a microelectromechanical system (MEMS) [143–145] metamaterial emitter (MME), which includes a metallic plate, a dielectric layer, and a free-standing top patterned metallic layer supported by a bimaterial (gold and silicon nitride) arm [146]. The ground plane is designed to

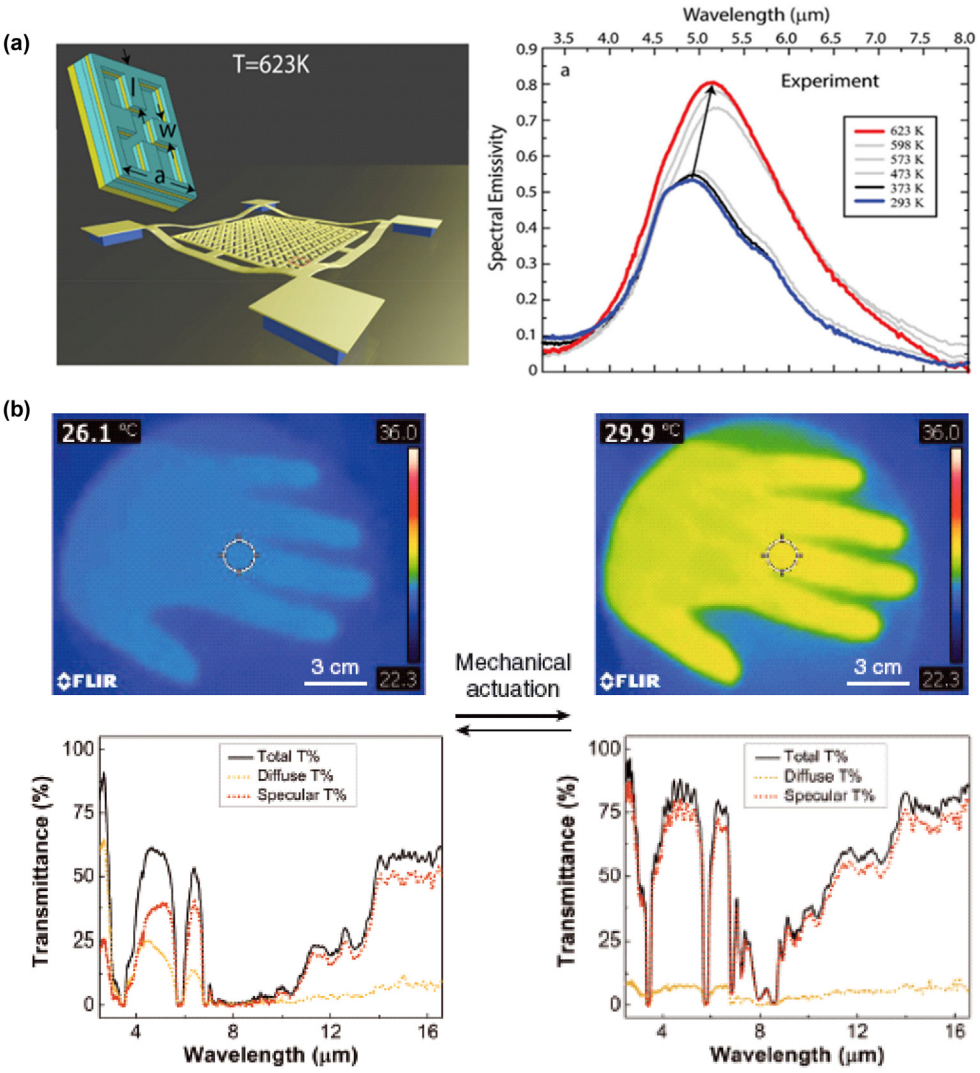

FIGURE 10

Strain-modulated materials for thermal camouflage. (a) Schematic of the self-driven device that responds to thermal strain and the experimental spectral emissivity at different temperature [146]. Copyright 2016, Wiley. (b) IR images and the corresponding spectral IR transmittance of the tri-layer structure for thermal camouflage by external mechanical actuation [147]. Copyright 2020, Wiley.

have relatively low emissivity at room temperature when the top layer is suspended. When heat is applied, the bimaterial arm will expand and bend down owing to different thermal expansion coefficients, resulting in the contact of the top and ground layers. The confluence of the electric and magnetic resonances on the feature geometry leads to the high emission state. The temperature-dependent spectral emissivity is shown in Fig. 10a. It is seen that at room temperature, the peak of the emissivity spectrum just over 0.5. With the increase of temperature to 623 K, the spectral emissivity monotonically increases to 0.81 at 5.2 μm. The merits of this metamaterial include the temperature-driven mechanical modulation and the distinct difference in emissivity spectra. Note that higher temperature leads to larger emissivity, which is contrary with most requirement for low-temperature thermal camouflage but can be applied for high-temperature thermal camouflage.

Above mechanical strain is exerted by self-driven thermal strain, while direct external mechanical actuation is more flexible and powerful to modulate the surface IR emissivity. Xu et al. sandwiched an acrylate elastomer layer with two sulfonated pentablock copolymer membranes by drawing inspiration from the dielectric elastomer actuators [147]. The elastomer has good elasticity and IR absorption, while the membranes are transparent to emit the elastomer's thermal radiation outside as much as possible. Without mechanical strain, the tri-layer structure is wrinkled with variable microscale roughness at about 564 nm; after applying mechanical strain, the tri-layer structure is flattened with surface roughness at about 15 nm. To demonstrate the potential thermal camouflage application, the authors put a warm hand below the tri-layer structure and observed the changes of the corresponding IR images. As shown in Fig. 10b, the wrinkled structure blocked the IR radiation of the hand largely with an average total transmittance of 27.6% and a high average total absorptance of 61.9%. After applying the mechanical strain, the flattened structure became more IR transparent with 53.5% in total transmittance and 33.1% in total absorptance in average. The mechanism for the change of IR transmittance and absorptance can be attributed to the variation of the

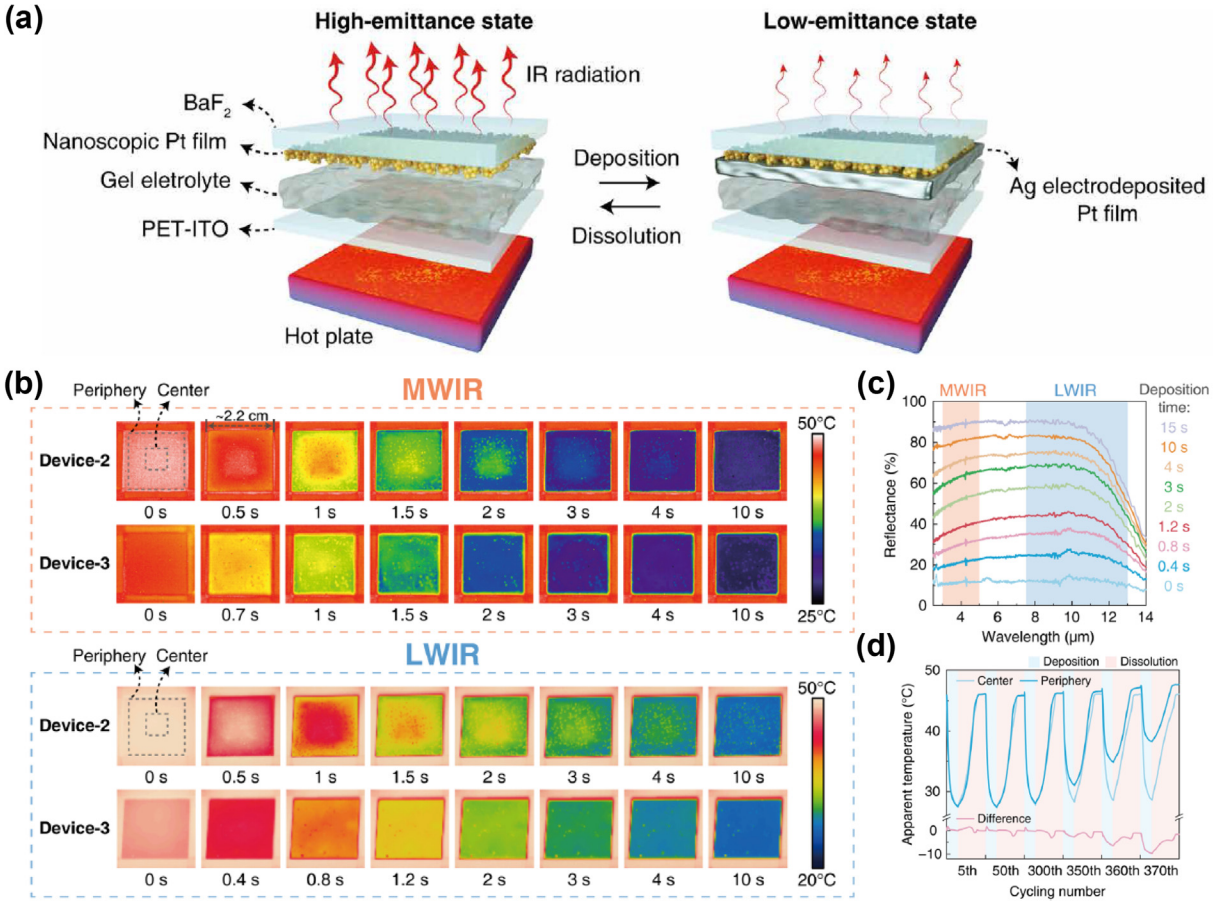

FIGURE 11

Chemical modulation for dynamic thermal camouflage. (a) Schematics of the nanoscopic Pt film-based reversible silver electrodeposition device at high- and low-emittance states by deposition or dissolution processes. (b) Real-time MWIR and LWIR images during the electrodeposition process. (c) Total reflectance spectral in the MWIR and LWIR ranges during the electrodeposition process. (d) Measured apparent temperature curves at different cycling tests at the central and peripherical regions [152]. Copyright 2020, AAAS.

thickness of the tri-layer structure and the surface roughness induced specular-to-diffuse performance. Such mechanical actuation could change the IR absorptance by almost two-fold and more importantly could be implemented reversibly. More than thermal camouflage, such system also exhibits potential in visible camouflage application with capability to transition from optically transparent to opaque states.

Chemical modulation

Chemicals have been long used to tune the surface emittance/reflectance in both the visible and IR spectra [148]. For example, hydrogen could be used to achieve the dynamic behavior of the plasmonic color display based on the unique hydrogenation/dehydrogenation kinetics of magnesium (Mg) nanoparticles [149]. Such chemical reversible transition between the metal Mg and dielectric magnesium hydride (MgH_2) alter the surface reflectance, allowing for the plasmonic color printing, color tuning, color erasing, and color restoration. Phan et al. fabricated a histidine-tagged reflectin coating, and found that the coating exhibited a large and reversible peak reflectance shift from 625 nm to 1200 nm, when exposed to acetic acid vapour [150]. As mentioned above, bulk metals, due to their high reflectance over the entire IR spectrum, are good candidates to suppress the thermal radiation, but using bulk metals for thermal camouflage is not perfect since the high reflectance may expose the targets. When reducing the size from bulk to microscale or even nanoscale, many new phenomena and physics on light-matter interactions are reported including thermal radiation, like surface plasmon polariton (SPP), localized SPP (LSPP), etc. At such scale, the surface absorption, reflection, transmission, and emission can be modulated in terms of the intensity, spectra, and directionality flexibly and significantly [151]. Li et al. presented a nanoscopic platinum (Pt) film-based device for dynamic thermal camouflage by modulating the silver (Ag) electrodeposition [152]. As shown in Fig. 11a, before the electrodeposition, the Pt film shows low reflectance and high emittance; after the electrodeposition, Ag will be gradually deposited on the Pt film and result in high reflectance and low emittance. It is the Ag film rather than the Pt film that can be dissolved and deposited, such high and low emittance states can be cycled to achieve the dynamic thermal radiation modulation. The thermal camouflage performance was evaluated by recording the real-time MWIR and LWIR images. As shown in Fig. 11b, after Ag deposition, the measured apparent temperature drops in both the MWIR and LWIR spectra with Pt film thickness of 2 and 3 nm (device-2 and device-3). Such temperature dropping corresponds to the state

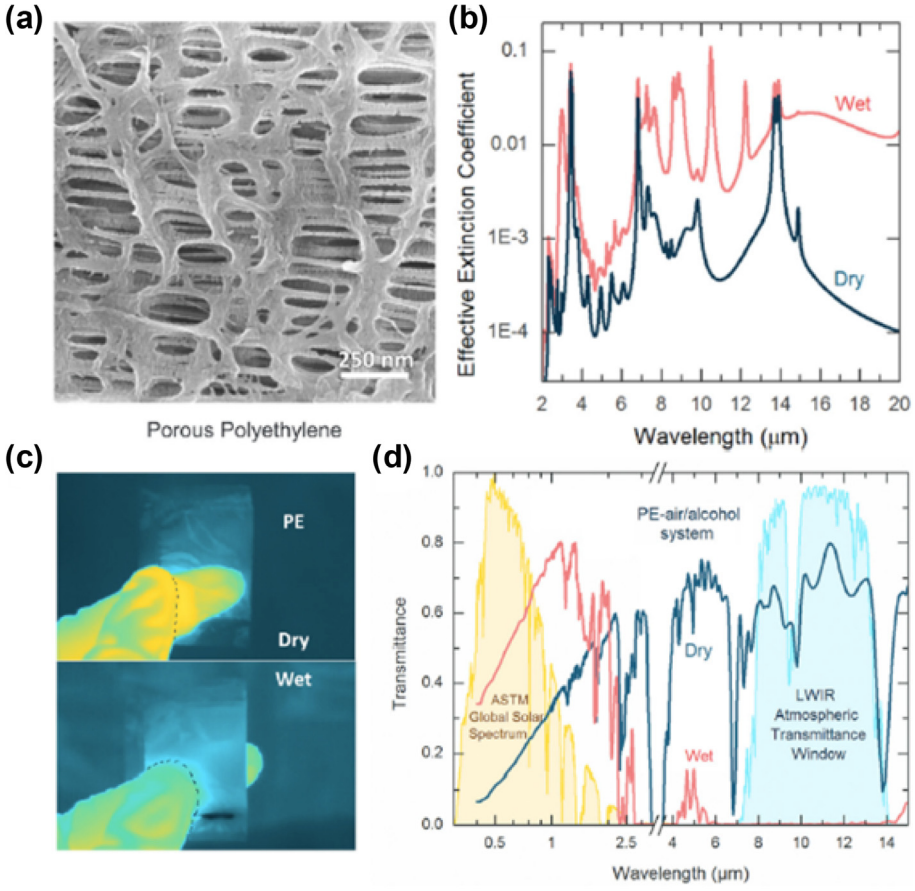

FIGURE 12

Wetting-modulated materials for thermal camouflage. (a) SEM of porous PE. (b) Effective electromagnetic extinction coefficients, (c) IR images, and (d) spectral transmittance of PE-air/alcohol PPC film at dry and wet states [118]. Copyright 2019, Elsevier.

transition from high emittance to low emittance in Fig. 11a, allowing the potential application for dynamic thermal camouflage. The corresponding total IR reflectance spectra are shown in Fig. 11c, and the maximum emittance tunability ranges in the MWIR and LWIR are as high as 0.77 and 0.71. The tunable stability and reversibility are also tested up to 350 cycles and shown in Fig. 11d. Moreover, they also demonstrated that the device could be enlarged and assembled, and suitable for rough and flexible substrates, and even compatible with structural color coating to extend the practical camouflage performance.

Wetting modulation

Some materials can also alter their optical properties by the humidity [153], like Poly(vinylidene fluoride-co-hexafluoropro pylene) (P(VDF-HFP)), poly tetra fluoroethylene (PTFE), ethyl cellulose, and polyethylene (PE) porous polymer coatings (PPCs) [154–156]. Based on these responsive PPCs, a wide range of applications has been proposed, including daylight regulation glass, tunable solar heating, radiative coolers, thermal management, and thermal camouflage [157–160]. Mandal et al. fabricated PE PPCs with porosity of ~40% and small pore size (~0.1 μm) to scatter IR wavelegnths, as shown in Fig. 12, resulting in high IR transmittance with low electromagnetic extinction coefficient [118]. When wetted with alcohols, the PE PPCs became IR absorptive and the effective extinction coefficient risen by ~10–100 times in the IR wavelength. The IR transmittance/emittance difference between the dry and wet states was 0.64. Such transition from transparent to opaque in IR wavelength enabled the promising applications for thermal camouflage. At dry state, the PE PPCs was IR transparent with high transmittance, and the finger behind the PE PPC film was observed. At wet state, the IR transmittance decreased and the film became opaque to camouflage the finger. Though wetting can be used to modulate the emissivity and thermal camouflage, but practical applications are still under investigation as the humidity is hard to control especially at outdoor scenarios.

Phase-changing materials

As mentioned above, thermal radiation of a black body is proportional to the fourth power of absolute temperature (T^4) according to the Stefan-Boltzmann law. The heat radiated by common materials is lower than that by timing a less-than-one integrated emissivity (ε_{int}) coefficient, which is independent or only weakly dependent on temperature in most materials (Fig. 13a) [161]. As a result, the common materials are hard to achieve thermal radiation modulation, let alone the dynamic thermal camouflage application. Phase-changing materials (PCMs), due to the dis-

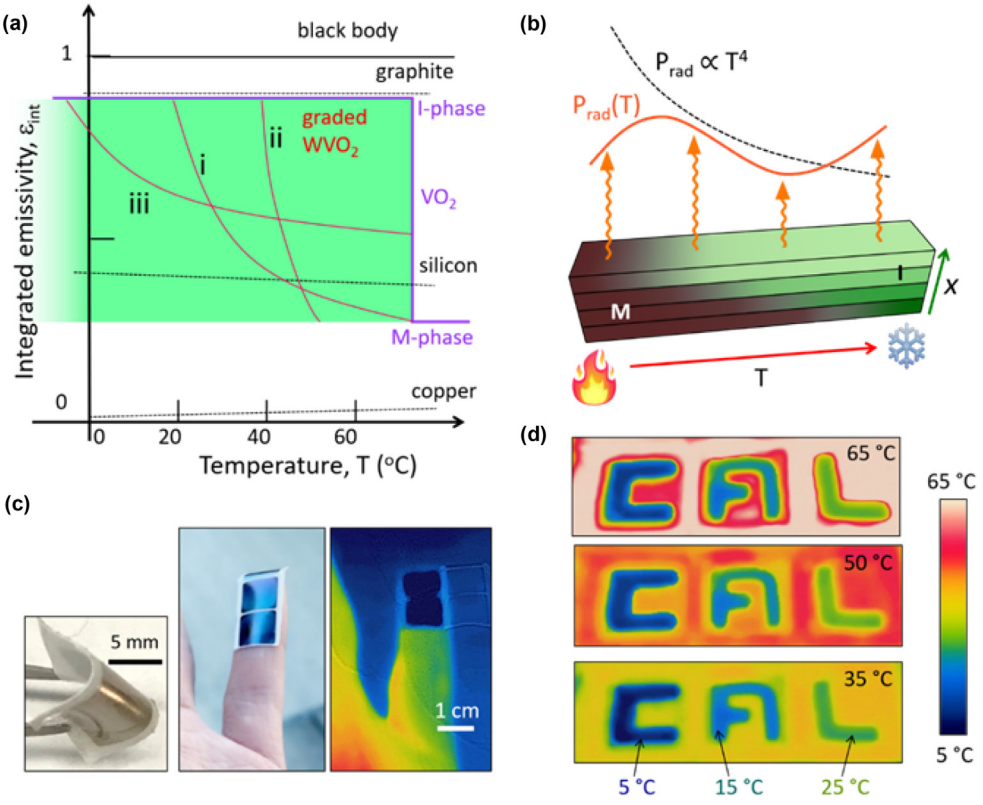

FIGURE 13

Thermal radiation modulation based on graded doped $W_xV_{1-x}O_2$. (a) Schematic illustrating realization of nearly arbitrary temperature dependence of integrated emissivity (ε_{int}) within the shaded area using graded $W_xV_{1-x}O_2$, represented by the three arbitrarily designed emissivity curves denoted by i, ii, and iii. (b) Schematic showing that by rational design of the W doping profile (x along thickness direction) of $W_xV_{1-x}O_2$, emissivity can be programmed to regulate thermal radiation (P_{rad}) for distinctly different behavior from the Stefan-Boltzmann T^4 law. (c) Optical image of an IR camouflage based on graded $W_xV_{1-x}O_2$ film transferred onto a PE tape, showing high mechanical flexibility. The fingertip is hidden from IR camera when covered with the camouflage. (d) Demonstration of T_{actual}-independent thermal IR decoy, a pattern of "CAL" is made to show "C" at constant $T_{IR} \approx 5$ °C, "A" at $T_{IR} \approx 15$ °C and "L" at $T_{IR} \approx 25$ °C, regardless of T_{actual} varying to 65, 50 or 35 °C [187]. Copyright 2020, Wiley-Blackwell.

tinct emissivity spectra at different phases, have also explored for thermal emission modulation and thermal camouflage [162–165]. For this end, vanadium oxide (VO_2) and $Ge_3Sb_2Te_6$ (GST) are the most frequently reported PCMs that can change their optical properties when achieving their phase transition temperatures [119,166–171].

VO_2 breaks the confinement of common materials due to the metal–insulator phase transition (MIT) at $T_{MIT} \sim 67$ °C [172], enabling an abrupt drop of ε_{int} at T_{MIT} for thermal radiation modulation. Due to its large negative differential thermal emissivity across the transition temperature [173], VO_2 shows great potential in emissivity engineering applications, like camouflage, smart windows, actuators, sensors, and thermoelectricity, etc [174–179]. Manipulating the MIT of VO_2 by external stimuli is an active field since VO_2 can be modulated not only by heat, but also by light, electricity, magnet, and stress, resulting in VO_2 as a promising candidate material for novel electronic and optical devices [180–184]. In addition, the MIT time for VO_2 is in picosecond scale with low thermal hysteresis and it even can be cycled over 10^6 times in terms of the MIT behavior, which is rather advantageous for dynamic thermal camouflage [185,186]. Moreover, tungsten (W) doped VO_2 (forming $W_xV_{1-x}O_2$) shifts MIT to any temperatures between ~0 °C and 67 °C depending on the W fraction x. However, in VO_2 or any uniformly doped $W_xV_{1-x}O_2$, the abrupt nature of the MIT limits applications of this property within a narrow temperature window (T < ~ 20 °C). Tang et al. overcame this limit by developing a thermal radiation modulation platform based on thin films of $W_xV_{1-x}O_2$ where x is judiciously graded along the thickness direction across a depth less than the skin depth of EM screening (~130 nm) at a broad temperature range from T_{MIT} (x_{max}) to T_{MIT} (x_{min}) [187]. This structure provides a materials platform for achieving nearly-arbitrary value and temperature dependence of emissivity by manipulating the x profile across the film thickness. Consequently, the surface thermal radiation is significantly different from the conventional T^4 law (Fig. 13b). Based on such a thermal radiation modulation platform, the thermal camouflage can be achieved. As demonstration, they first made a thermal camouflage film by programming ε_{int} to obey an inverse dependence on T^4, giving the rather cool temperature even on a hot finger (Fig. 13c). The fabricated camouflage film is power-free, mechanically flexible, and has unprecedented advantages such as inherent immunity to intensive spatial variation and temporal fluctuation of temperature. They further developed a unique function named a thermal "decoy" to passively conceal objects in the IR camera and even generate a counterfeited tem-

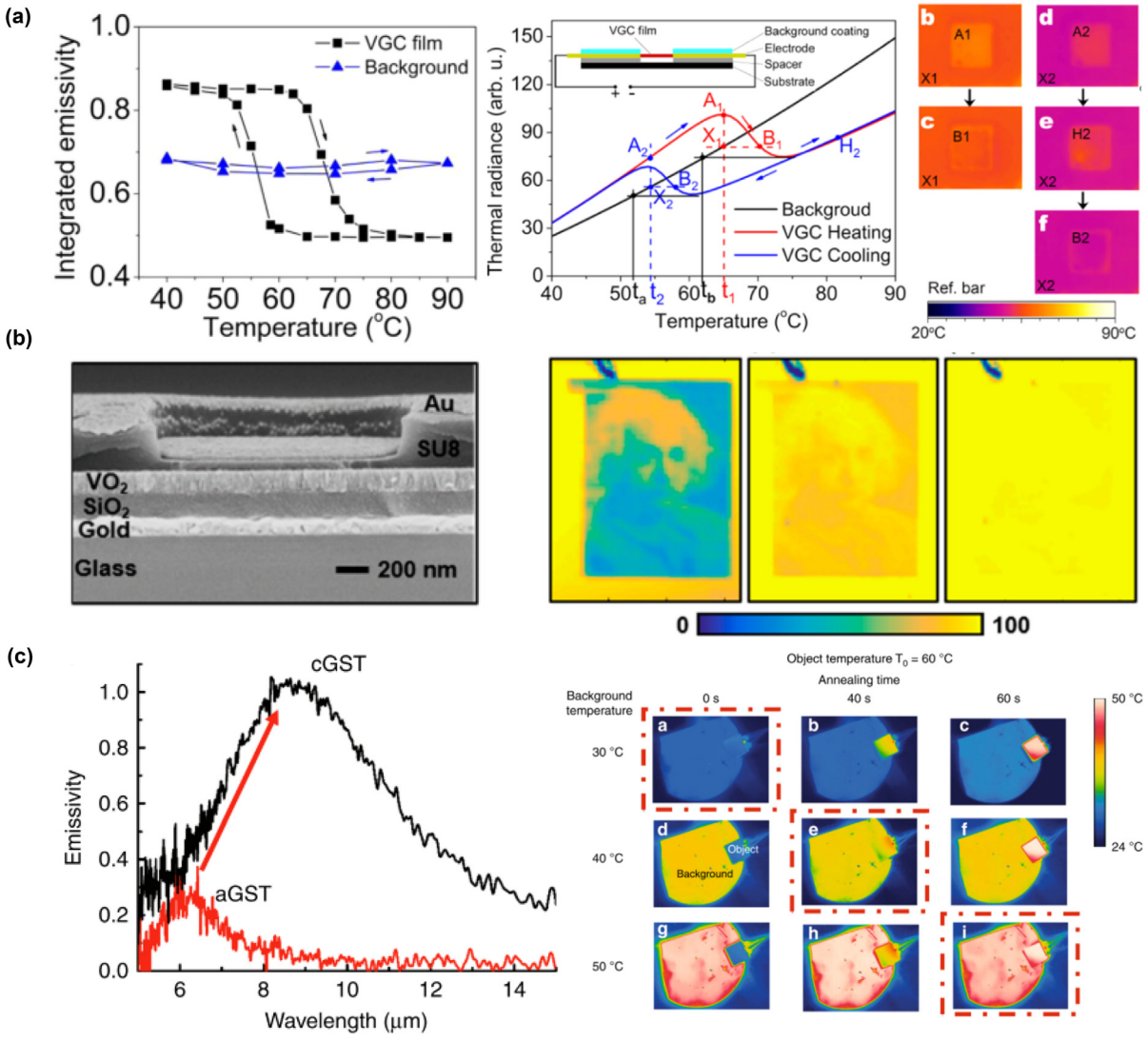

FIGURE 14

Emissivity-modulated PCMs for thermal camouflage. (a) Temperature-dependent emissivity and thermal radiance of the VO_2/graphene/CNT (VGC) film [119]. Copyright 2015, American Chemical Society. (b) TEM and FTIR scan generated images for the VO_2-based plasmonic surface [16]. Copyright 2018, American Chemical Society. (c) Emissivity spectrum comparison of the crystalline and amorphous phases of GST and the related thermal camouflage performance [192]. Copyright 2018, Nature Publishing Group.

perature. A working decoy is demonstrated in Fig. 13d, where the image of "CAL" shows a stable temperature when the background temperature changes from 35 to 65 °C.

Based on MIT properties of VO_2, many other thermal camouflaging metamaterails are also reported. Xiao et al. reported another adaptive thermal camouflage system based on a VO_2/-graphene/CNT (VGC) sandwich-like structure [119]. In the structure, VO_2 is used for IR emission regulation, and CNT and graphene layers are used to mechanical framework to support and ensure the uniform VO_2. The integrated emissivity was characterized by modifying the preset emissivity of the IR camera until the detected temperature equals to that of the calibrated thermocouple. It is seen that the background emissivity is nearly independent on temperature, while that of the VGC shows apparent negative differential emissivity ranges from 0.86 to 0.49 at a temperature range from 40 to 90 °C. Due to the emissivity hysteresis, the thermal radiance from the VGC film undergoes different paths during heating and cooling, as shown in Fig. 14a. Due to the negative thermal emissivity, though the temperature of B_1 is larger, A_1 looks hotter. When VGC is heated from A_2, H_2 to B_2, the background emits the same thermal radiance, and B_2 is blend into the background at the cooling path. Chandra et al. combined VO_2 with an imprinted plasmonic surface to achieve adaptive thermal camouflage by utilizing the localized surface plasmon resonance (LSPR) of the plasmonic surface at a given frequency in the MWIR and LWIR bands [16]. The multilayer cavity-coupled plasmonic structure, as shown in Fig. 14b, consists of a gold hole/disk array, a SiO2/VO_2/polymer cavity spacer and a reflective back mirror. Through FDTD simulations, the so-called Fabry-Perot assisted LSPR was observed, and the

absorption peak is blue shifted with the increase of the temperature above 330 K. The IR-coded Albert Einstein image is clearly seen for at 295 K (insulate VO_2), and becomes ambiguous and even invisible at 320 K (phase-separated VO_2) and 360 K (metallic VO_2) respectively, demonstrating the thermal camouflage function of VO_2 with temperature. Note that the unpleasant color of VO_2 will negatively restrict its application to camouflage and VO_2 will be oxidized into toxic V_2O_5 at higher temperature, which will deteriorate its camouflage performance. It may be a solution to coat the VO_2 with the core–shell structure to improve the anti-oxidation and visible properties. The desired shell materials range from SiO_2, TiO_2, and ZnS, which have high visible or IR transmittance. To decrease the transition temperature, VO_2/carbon hybrid PCM was reported via plasma enhanced chemical vapor deposition. The thermal emissivity contrast is as high as 0.44 and the transition temperature is lowered to 45 °C.

Unlike VO_2-based metamaterials, GST alloys undergo the phase transition from amorphous to crystalline states, exhibiting different thermal emission characteristics [188–191]. Owing to the different atomic configuration, the imaginary part of the relative permittivity of the amorphous GST (aGST) is negligible, while that of the crystalline GST (cGST) increases with the wavelength. As a result, aGST is transparent while cGST is highly absorptive in the mid-IR band, leading to the distinct difference in emissivity spectrum. Qu et al. fabricated a GST-Au double-layered film, whose emissivity spectra were measured and shown in Fig. 14c [192]. It is seen that aGST-Au film has a rather lower emissivity compared to cGST-Au film, which is because of the absence of resistive loss in the aGST layer to contribute to the thermal emission. It is perceived that the emissivity of the intermediate phase is in between due to the coexistence of both aGST and cGST phases simultaneously. As a result, the thermal emission will be enhanced greatly when changing from aGST phase to cGST phase by controlling the annealing time. The thermal camouflage effect is achieved when the radiation temperature of the aGST-Au film approximates to that of the background at 30 °C, but when the background temperature is increased (40 °C or 50 °C for example), the aGST-Au film is identified since the apparent radiation temperature is still 30 °C without changing the emissivity spectrum. By enhancing the annealing time, the aGST phase changes to cGST phase gradually with increased emissivity, and the GST-Au film achieves good thermal camouflage again when the apparent radiation temperatures of the GST-Au film and the background approximate. For example, after annealing for 40 s (60 s) for the GST, the GST-Au film at 60 °C can be camouflaged in the 40 °C (50 °C) background again. What's more, the robustness of thermal camouflage function was further validated by changing the observation angle from 0° to 60°, confirming that the emissivity spectrum is insensitive to the observation angles. Even though, the practical application of GST for thermal camouflage is still under exploring as the annealing temperature is high and the annealing process is lacking in practices. Compared to VO_2, GST-based metamaterials are usually challenged by their relatively larger thermal hysteresis, which may limit the dynamic thermal camouflage characteristics. Note that the background temperature is usually changing slowly, thus in some situations, GST-based metamaterials, though limited, may find their proper applications. Actually, there have existed some hysteresis-free MIT PCMs in rare-earth nickelates with very high MIT temperatures [193,194]. Among them, samarium nickel oxide ($SmNiO_3$) is a typical example, which exhibits an extraordinary temperature-driven fully reversible and hysteresis-free MIT process [195]. Its thermal emissivity is found to follow a unique temperature dependence T^{-4}, resulting in that the thermal radiation energy remains constant over a wide range of temperature against the traditional Stefan-Boltzmann law. This is of course extremely hard to achieve by conventional materials. Such properties seem suitable for potential thermal camouflage against the temperature change of the objects and over a wide temperature range, but the high MIT temperature remains challenging for practices.

Other than MIT-based PCMs, the conventional PCMs can also be applied for thermal camouflage, not due to their dynamic emissivity but owing to their large latent heat storage properties with constant temperature [162,165,170,175,188,189]. Lyu et al. propose to integrate Kevlar nanofiber aerogel (KNA) film with PCM fillers to achieve thermal camouflage function [2]. The obtained KNA film are flexible, foldable and robust with high porosity and specific surface area, making it easy to embed PCM fillers, Polyethylene glycol (PEG). The working principle of the KNA/PCM film for achieving thermal camouflage is shown in Fig. 15a. The KNA/PCM film will delay the temperature rise at daytime and temperature drop at nighttime by its phase transition process, making the target blending in the background in an IR camera. With incident sunlight, the target is detected due to the higher radiant temperature than the KNA/PCMs and the background, and the average temperature difference between the latter two is less than 0.5 °C. Without incident sunlight, the large temperature change of the target makes it detectable, whereas the KNA/PCM is blended into the background as well. When the target is covered by the KNA/PCM film, it is invisible without large temperature change. Further, when the targets generate heat continuously, the covered KNA/PCM will be heated up eventually, leading to the deterioration of the thermal camouflage function. Possible solutions to this issue can be achieved by increasing the thickness or layer number of the KNA/PCM films, or by resorting to the combined structure of KNA and KNA/PCM films to disturb the IR propagation toward detectors. Ahn et al. developed a thermal camouflage textile with polyurethane (PU) -tin oxide (SnO_2) composite microtubes [18]. Due to the relatively high refractive index of SnO_2 (~1.9), the reflectance of the composite increases with the content of SnO_2. As a result, IR rays above 2.5 μm cannot be transmitted through the composite, leading to the low external IR radiation and the thermal insulating properties. The schematic for the working performance is shown in Fig. 15b, in which water is repellent and IR radiation is blocked. The thermal camouflage function is clearly demonstrated through comparative experiments. Though the target tank with heat generation, the target is camouflage and concealed into the background after covering with the PU-SnO_2 textile. Further, the thermal camouflage performance is improved by filling the microtubes with PCMs, like paraffin oil and water.

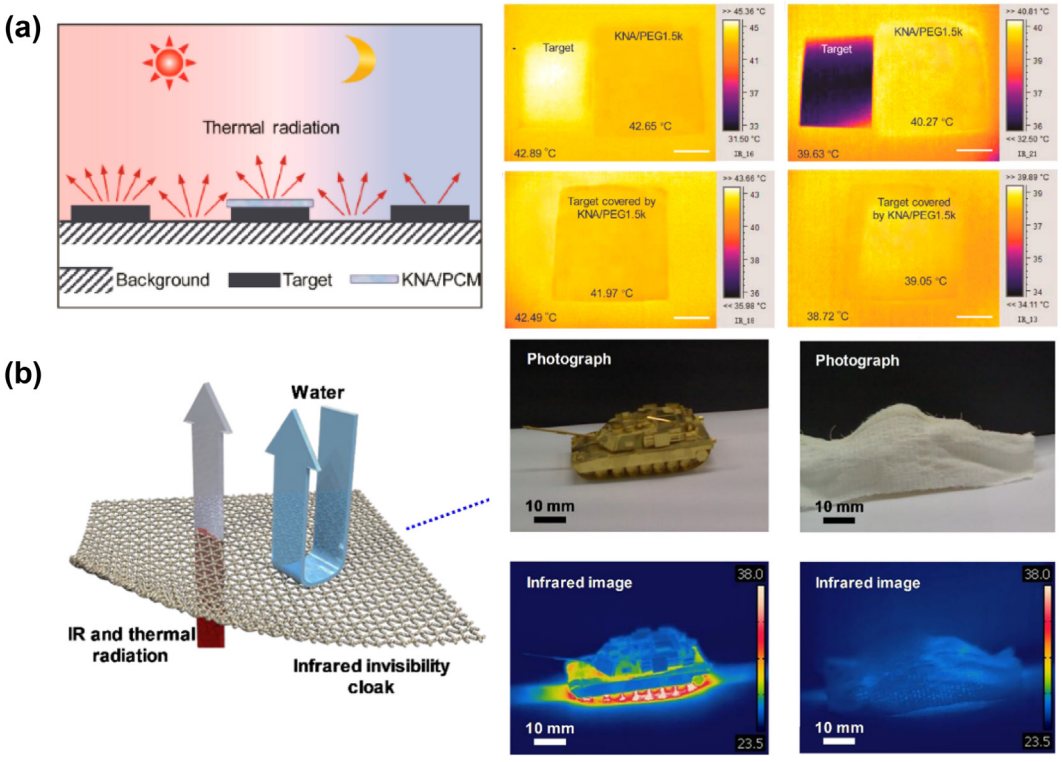

FIGURE 15

Temperature-modulated PCMs for thermal camouflage. (a) Working schematic for Kevlar nanofiber Aerogel (KNA) and PCM composite, and the IR experiments [2]. Copyright 2019, American Chemical Society. (b) Schematic of the fabricated textile with the IR- and thermal radiation insulation and water-repellent properties, and comparative IR experiments to show the thermal camouflage performance [18]. Copyright 2019, American Chemical Society.

Bio-inspired materials

The most well-known camouflage masters in nature are the cephalopods and chameleon, which can dynamically change the color of their skins to adapt for the change of environment [196,197]. Inspired by these camouflage masters, many camouflage-related technologies have been developed including, but not limited to, real-time active full-visible color mechanical chameleon camouflage [198], adaptive multiplexed optoelectronic camouflage system[3], soft-machine-based camouflage and display [199–202], electrical-stimulated dielectric elastomers [203–206]. Note that most of these natural camouflage examples only refer to the visible band, while for thermal camouflage, the IR band should be covered in terms of the absorptivity (emissivity) or reflectivity spectrum. Gorodetsky and colleagues develop many different strategies to achieve thermal camouflage by drawing inspiration from the natural world [207–212]. They, inspired by the reflectin platelets in iridophores, developed the protein-based color-changing coatings to achieve reconfigurable thermal camouflage [150]. The ambient acetic acid vapor could induce substantial swelling owing to the change in intra-protein electrostatic interactions, so as to modulate the surface reflectivity spectrum. Further, they fabricated the reflectin film on graphene oxide-coated fluorinated ethylene propylene tape, which shows mechanical tunability of reflectivity spectrum and potential for thermal camouflage [196]. Recently, they drew inspiration from the skin of coleoid cephalopods in terms of the patterning and coloration characteristics, and developed adaptive IR-reflecting platforms that can be modulated under electrical and mechanical stimuli [213]. As shown in Fig. 16a, they prepared a device with aluminum-coated active area in the shape of a swimming squid's silhouette and observed through an IR camera. After electrical actuation, the squid silhouette-shaped device became flat, and the decrease in the reflectivity spectrum make the device hotter in the IR camera. Cui et al. inspired by polar bear hairs and succeeded in weaving large-scale fibers with aligned porous structure into biomimetic textile with excellent properties of thermal insulation, breathability, and wearability [214]. Due to the super thermal insulation property of the biomimetic textile, when covered with, the target with heat sources, such as the rabbit body as shown in Fig. 16b, can be concealed in the IR camera, demonstrating to be a good candidate for thermal camouflage materials. They further discussed that the thermal camouflage performance can be accessed in a wide range of environment temperature from −10 to 40 °C. The mechanism is attributed to the aligned porous structure of the biomimetic fiber, which suppresses the thermal convection and conduction and improves the reflectance of IR light due to the "multiple reflective effect", resulting in the favorable thermal insulation property and low-temperature thermal camouflage performance.

Perspectives and concluding remarks

Inspired by the camouflage creatures in nature, camouflage-related technologies in multiple disciplines have been developed and explored. Among them, thermal camouflage has captured intensive attention in recent decades, owing to its increasing importance in the military applications and the indirect thermal

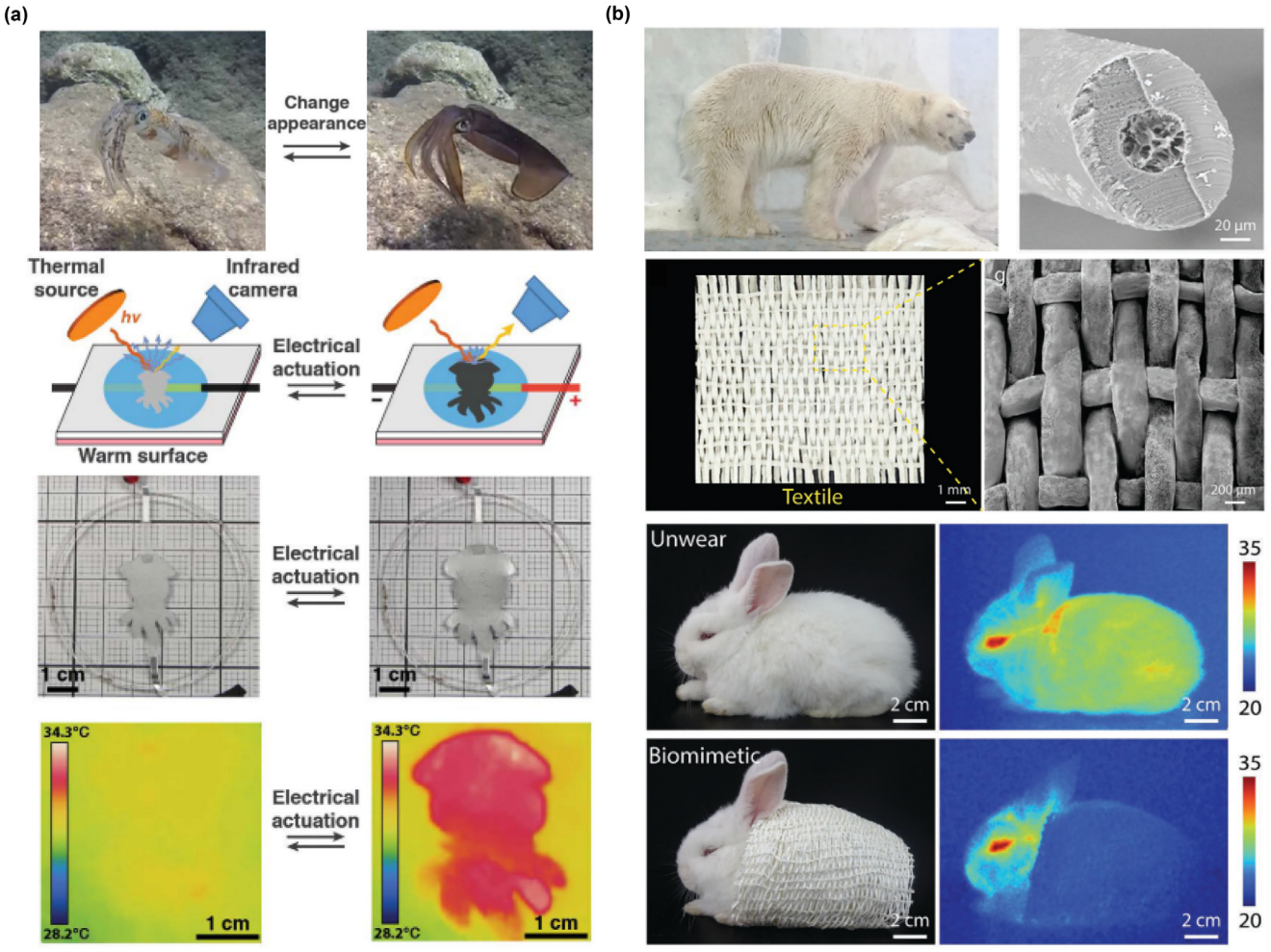

FIGURE 16

Bio-inspired materials for thermal camouflage. (a) Cephalopod-inspired IR-reflecting platform with electrical actuation [213]. Copyright 2018, American Association for the Advancement of Science. (b) Polar bear hair inspired biomimetic textile with super thermal insulation property [214]. Copyright 2018, Wiley-Blackwell.

management applications derived from its working principle. The working mechanisms of the thermal camouflage can be categorized into conductive and radiative thermal camouflage. The former one is to change the surface temperature or to achieve thermal illusions near the target so as to achieve thermal camouflage, and the in-plane and out-of-plane conductive camouflage technologies are reviewed. Nevertheless, due to the intrinsic limitations such as relatively slow heat conduction, existence of contact resistance, and presence of heat source's influence, the conductive thermal camouflage exhibits limitations in practical camouflaging applications. As a counterpart, the radiative thermal camouflage could be very robust and viable, while the emissivity spectrum should be selectively and judiciously considered. The emissivity-engineered thermal camouflage and multispectral camouflage technologies are introduced. Moreover, since the environment may change and targets would move, the dynamically modulated materials based (e.g. electrical, optical, strain, wetting, phase-changing, bio-inspired materials) radiative thermal camouflage technologies are presented and reviewed. Along the roadmap of thermal camouflage technologies, the adaptive or intelligent thermal camouflage technologies, such as chameleon-like smart camouflage, are surely along the development roadmap of this field. Though it is still challenging as of now, there are a few promising ways toward it.

- The first approach is the temperature-responsive emissivity engineering, which is more practical for adaptive thermal camouflage than the electricity-, light-, chemical-, wetting-, and mechanics-modulated emissivity. Thermal radiation is determined by both surface emissivity and temperature, and the latter is more sensitive due to the fourth-power dependence. Ideal emissivity spectra are desired as perfect thermal camouflage needs efficient thermal management solutions simultaneously. The reported temperature-stimulated phase-changing materials, such VO_2 and GST, may be utilized but not limited to them, due to their different and narrow phase

transition temperature. Other PCMs with broad phase transition temperature or hierarchical PCM composites should be explored to enhance the applicability of thermal camouflage.

- The second approach is to employ the soft materials with desired thermal emission characteristics. Compared with rigid materials, soft materials could cover objects in arbitrary, thus the potential applications may be greatly enhanced. Such materials could in the form of film, solution, gel, fiber, etc. They may be conformally coated, sprayed, and wrapped onto the targets' surfaces of arbitrary sizes and shapes, and they also may be woven or knitted into textile for wearable application. To design such composite materials with desired thermal camouflage performance is rather challenging. As discussed before, the ideal emissivity spectra of thermal camouflage are the opposite to those for radiative cooling. Thus, it is rather confidential that the inverse design of such composite materials has been implemented successfully for radiative cooling soft materials in various forms like film [215], coating [216], fiber/textile [156,217,218].
- The third approach is the multispectral camouflage engineering, such as camouflage technologies in IR and microwave wavelength ranges, in IR and visible wavelength ranges, or even in the full-wavelength range. The multispectral camouflage, superior to single-spectral camouflage, can achieve practical camouflage performance against the developing multispectral detection technologies nowadays. Although it is becoming aware about the importance of the multispectral camouflage, it still rather challenging. The reported hierarchical metamaterials based on multilayer structures shows one possibility [116], and there is still plenty of room toward this goal in terms of design, fabrication, and practical application. There has come a consensus that the camouflage technologies and the detection technologies are competing along the development, but the former one lags behind the latter and thus more effort are demanded.
- The last but not the least is the detection-feedback method. We can use the detected thermal emission from the background as the input to adjust dynamically the surface's thermal emission for thermal camouflage. Such detection-feedback system may be complicated and involve opto-/electronic modules, control circuits, and signal process units. The exploration of adaptive or intelligent thermal camouflage refers to multi-discipline interactions of thermotics, physics, optics, mechanics, electronics, and materials, and the corresponding system integration and compactness need further investigation.

Declaration of Competing Interest

The authors declare that they have no known competing financial interests or personal relationships that could have appeared to influence the work reported in this paper.

Acknowledgements

R. H. would like to acknowledge the financial support by National Natural Science Foundation of China (No. 52076087, and No. 51625601), and the Applied Basic Frontier Programs of Wuhan City (No. 2020010601012197). C.-W.Q. acknowledged the financial support by Ministry of Education, Republic of Singapore (No.: R-263-000-E19-114).

Data Availability

Data can be requested from the corresponding authors upon reasonable request.

References

[1] R. Fleury, A. Alu, Prog. Electromagn. Res. 147 (2014) 171–202.
[2] J. Lyu et al., ACS Nano 13 (2019) 2236–2245.
[3] C.J. Yu et al., Proc. Natl. Acad. Sci. USA 111 (2014) 12998–13003.
[4] D. Franklin et al., Light-Sci. Appl. 7 (2018) 93.
[5] S.C. Dang et al., Mater. Res. Express 6 (2019) 106422.
[6] Y. Li et al., Nat. Commun. 9 (2018) 273.
[7] J. Mei et al., Nat. Commun. 3 (2012) 756.
[8] M. Yang, P. Sheng, Annu. Rev. Mater. Res. 47 (2017) 83–114.
[9] N. Gao, K. Lu, Appl. Acoust. 169 (2020) 107500.
[10] P. Bermel et al., Opt. Express 18 (2010) A314–A334.
[11] S. Hong et al., Adv. Funct. Mater. 30 (2020) 1909788.
[12] F.P. Lang et al., Int. J. Thermophys. 39 (2018) 6.
[13] S. Bauer et al., Adv. Mater. 26 (2014) 149–161.
[14] P.C. Li et al., Adv. Funct. Mater. 29 (2019) 1901908.
[15] S.A. Morin et al., Science 337 (2012) 828–832.
[16] S. Chandra et al., ACS Photonics 5 (2018) 4513–4519.
[17] T.C. Han et al., Adv. Mater. 26 (2014) 1731–1734.
[18] J. Ahn et al., ACS Appl. Mater. Inter. 11 (2019) 14296–14304.
[19] M.J. Moghimi et al., Adv. Eng. Mater. 20 (2018) 1800038.
[20] L. Peng et al., Adv. Opt. Mater. 6 (2018) 1801006.
[21] F. Sibille, Rep. Prog. Phys. 49 (1986) 1197–1242.
[22] M. Razeghi, B.M. Nguyen, Rep. Prog. Phys. 77 (2014) 082401.
[23] T. Han, C.W. Qiu, J. Opt. 18 (2016) 044003.
[24] C. Amra et al., Proc. R. Soc. A-Math. Phys. 471 (2015) 20150143.
[25] F. Chen, D.Y. Lei, Sci. Rep. 5 (2015) 11552.
[26] T.C. Han et al., Sci. Rep. 5 (2015) 10242.
[27] S. Narayana et al., Appl. Phys. Lett. 102 (2013) 201904.
[28] C.Z. Fan et al., Appl. Phys. Lett. 92 (2008) 251907.
[29] G. Gbur, Opt. Lett. 40 (2015) 986–989.
[30] L. Zhou et al., Phys. Lett. A 383 (2019) 759–763.
[31] W.X. Jiang et al., Phys. Rev. E 77 (2008) 066607.
[32] R. Hu et al., Epl-Europhys. Lett. 111 (2015) 54003.
[33] U. Leonhardt, Nature 499 (2013) 418.
[34] Y. Liu et al., Phys. Lett. A 383 (2019) 2296–2301.
[35] R. Hu et al., Chin. Phys. Lett. 33 (2016) 044401.
[36] L.Z. Wu, J. Heat Transfer ASME 137 (2015) 021301.
[37] Y.G. Ma et al., Phys. Rev. Lett. 113 (2014) 205501.
[38] R. Fleury et al., Phys. Rev. Appl 4 (2015) 037001.
[39] Q.W. Hou et al., Appl. Phys. Lett. 109 (2016) 103506.
[40] T.Z. Yang et al., Adv. Mater. 27 (2015) 7752–7758.
[41] S. Zhou et al., Int. J. Heat Mass Tran. 127 (2018) 607–613.
[42] J. Wang et al., Sci. Rep. 7 (2017) 7541.
[43] W. Sha et al., J. Appl. Phys. 128 (2020) 045106.
[44] X. He, L.Z. Wu, Appl. Phys. Lett. 105 (2014) 221904.
[45] R. Hu et al., Adv. Mater. 30 (2018) 1707237.
[46] Y. Li et al., Phys. Lett. A 380 (2016) 1641–1647.
[47] T.Y. Chen et al., J. Appl. Phys. 117 (2015) 054904.
[48] S. Narayana, Y. Sato, Phys. Rev. Lett. 108 (2012) 214303.
[49] N.A. Pfiester, T.E. Vandervelde, Phys. Status Solidi A-Appl. Mater. 214 (2017) 1600410.
[50] A. Rogalski et al., J. Appl. Phys. 105 (2009) 091101.
[51] Y.C. Liu et al., Opt. Express 24 (2016) 5683–5692.
[52] R. Hu et al., Phys. Rev. Appl 10 (2018) 054032.
[53] R. Hu et al., AIP Adv. 6 (2016) 125111.
[54] R. Hu et al., Adv. Mater. 31 (2019) 1807849.
[55] L.J. Xu et al., Eur. Phys. J. B 91 (2018) 166.
[56] Y. Li et al., Phys. Rev. Lett. 115 (2015) 195503.
[57] Q. Ji et al., Int. J. Mod Phys B 32 (2018) 1840004.
[58] X.Y. Shen, J.P. Huang, Int. J. Heat Mass Tran. 78 (2014) 1–6.
[59] R. Wang et al., J. Appl. Phys. 123 (2018) 115117.
[60] A.j. Minnich et al., Nanosc. Microsc. Therm. 20 (2016) 1–21.
[61] B.Y. Balagurov et al., J Exp. Theor. Phys. 112 (2011) 327–332.

[62] R. Schittny et al., Phys. Rev. Lett. 110 (2013) 195901.
[63] M. Farhat et al., Sci. Rep. 5 (2015) 9876.
[64] L. Xu, J. Huang, Int. J. Heat Mass Transfer 159 (2020) 12013.
[65] T.C. Han et al., Phys. Rev. Lett. 112 (2014) 054302.
[66] G. Fujii et al., Appl. Phys. Lett. 112 (2018) 061108.
[67] G. Fujii, Y. Akimoto, Appl. Phys. Lett. 115 (2019) 174101.
[68] S.R. Sklan, B.W. Li, Natl. Sci. Rev. 5 (2018) 138–141.
[69] E.M. Dede et al., Appl. Phys. Lett. 103 (2013) 63501.
[70] H.S. Choe et al., Nano Lett. 19 (2019) 3830–3837.
[71] X. Zhang et al., Chin. Phys. B 28 (2019) 064403.
[72] P. Xiayao, H. Run, ES Energy Environ. 6 (2019) 39–44.
[73] L.J. Xu, Eur. Phys. J. B 90 (2017) 221.
[74] Y.G. Peng et al., Adv. Funct. Mater. 30 (2020) 2002061.
[75] J. Zhang et al., Chin. Phys. Lett. 38 (2021) 010501.
[76] L. Zhao et al., Nanomaterials 9 (2019) 1096.
[77] H. Bu et al., Opt. Mater. 84 (2018) 109–114.
[78] H. Ji et al., Sol. Energy Mater. Sol. C 175 (2018) 96–101.
[79] L. Miao et al., J. Appl. Spectrosc. 83 (2017) 1102–1106.
[80] G. Tagliabue et al., Sci. Rep. 4 (2014) 7181.
[81] H. Demiryont, D. Moorehead, Sol. Energy Mater. Sol. C 93 (2009) 2075–2078.
[82] O. Salihoglu et al., Nano Lett. 18 (2018) 4541–4548.
[83] L. Cai et al., Adv. Mater. 30 (2018) e1802152.
[84] L.P. Wang, Z.M. Zhang, Appl. Phys. Lett. 100 (2012) 063902.
[85] Z.Y. Yang et al., ACS Photonics 4 (2017) 2212–2219.
[86] A. Sakurai et al., ACS Central. Sci. 5 (2019) 319–326.
[87] F. Le et al., ACS Nano 2 (2008) 707–718.
[88] Z.Y. Wang et al., ACS Photonics 5 (2018) 2446–2452.
[89] K. Ikeda et al., Appl. Phys. Lett. 92 (2008) 021117.
[90] Z. Zhou et al., J. Nanophotonics 10 (2016) 016014.
[91] B. Auguie et al., J. Opt. 17 (2015) 035003.
[92] C. Gmachl et al., Rep. Prog. Phys. 64 (2001) 1533–1601.
[93] J. Luo, Y. Lai, Opt. Express 27 (2019) 15800–15811.
[94] H. Zhu et al., Light-Sci. Appl. 9 (2020) 60.
[95] Z. Han et al., IEEE Photon. Tech. Lett. 19 (2007) 91–93.
[96] P. Neutens et al., Nat. Photonics 3 (2009) 283–286.
[97] M.T. Hill et al., Opt. Express 17 (2009) 11107–11112.
[98] J.L. Song et al., Opt. Express 28 (2020) 875–885.
[99] Y. Liu et al., Nanophotonics 9 (2020) 0485.
[100] J.K. Zhang et al., Opt Mater. Express 9 (2019) 195–202.
[101] S.M. Zhong et al., Opt. Express 26 (2018) 16466–16476.
[102] K. Wang et al., J. Alloys Compd. 690 (2017) 741–748.
[103] D. Qi et al., Materials 11 (2018) 1594.
[104] M.Y. Pan et al., Nano Energy 69 (2020) 104449.
[105] X. Feng et al., Opt. Express 28 (2020) 9445–9453.
[106] D. Qi et al., Opt. Lett. 43 (2018) 5323–5326.
[107] J. Lee et al., Adv. Funct. Mater. 30 (2020) 2003028.
[108] C. Zhang et al., Adv. Mater. Technol.-US 4 (2019) 1900063.
[109] H. Tian et al., Chin. Phys. B 23 (2014) 025201.
[110] S.N. Huang et al., J Phys. D-Appl. Phys. 54 (2021) 015001.
[111] Q.C. Wang et al., Infrared Phys. Technol. 79 (2016) 144–150.
[112] J. Ran et al., Ind. Eng. Chem. Res. 56 (2017) 10667–10677.
[113] A. Teber et al., J. Magn. Magn. Mater. 406 (2016) 228–232.
[114] O. Balci et al., Nat. Commun. 6 (2015) 6628.
[115] S.M. Zhong et al., Appl. Phys. Lett. 110 (2017) 063502.
[116] T. Kim et al., Adv. Funct. Mater. 29 (2019) 1807319.
[117] T. Inoue et al., Nat. Mater. 13 (2014) 928–931.
[118] J. Mandal et al., Joule 3 (2019) 3088–3099.
[119] L. Xiao et al., Nano Lett. 15 (2015) 8365–8370.
[120] Z.J. Coppens, J.G. Valentine, Adv. Mater. 29 (2017) 1701275.
[121] S. Vassant et al., Phys. Rev. Lett. 109 (2012) 237401.
[122] S. Vassant et al., Appl. Phys. Lett. 102 (2013) 081125.
[123] V.W. Brar et al., Nat. Commun. 6 (2015) 7032.
[124] T. Inoue et al., Phys. Rev. B 91 (2015) 235316.
[125] J. Park et al., Sci. Adv. 4 (2018) eaat3163.
[126] G.R. Bhimanapati et al., ACS Nano 9 (2015) 11509–11539.
[127] C.N.R. Rao et al., Angew. Chem. Int. Ed. 48 (2009) 7752–7777.
[128] C. Tan et al., Chem. Rev. 117 (2017) 6225–6331.
[129] A.H. Castro Neto et al., Rev. Mod. Phys. 81 (2009) 109–162.
[130] F. Bonaccorso et al., Science 347 (2015) 1246501.
[131] G.V. Naik et al., Adv. Mater. 25 (2013) 3264–3294.
[132] J. Chen et al., Nature 487 (2012) 77–81.
[133] Z. Fei et al., Nature 487 (2012) 82–85.
[134] L. Ju et al., Nat. Nanotechnol. 6 (2011) 630–634.
[135] F.H.L. Koppens et al., Nat. Nanotechnol. 9 (2014) 780–793.
[136] M.S. Dresselhaus et al., Adv. Mater. 19 (2007) 1043–1053.
[137] A.I. Hochbaum et al., Nature 451 (2008) 163–165.
[138] R. Venkatasubramanian et al., Nature 413 (2001) 597–602.
[139] L.E. Bell, Science 321 (2008) 1457–1461.
[140] B. Poudel et al., Science 320 (2008) 634–638.
[141] S. Hong et al., Adv. Funct. Mater. 30 (2019) 1909788.
[142] Y.Z. Xiao et al., Light-Sci. Appl. 8 (2019) 51.
[143] M. Liu et al., Fast Tunable Terahertz Absorber Based on a MEMS-driven Metamaterial, Conference on Lasers and Electro-Optics, OSA Technical Digest, Optical Society of America, 2017, pp FM1G.5..
[144] X.L. Liu, W.J. Padilla, Adv. Opt. Mater. 1 (2013) 559–562.
[145] X.Y. Liu, W.J. Padilla, Optica 4 (2017) 430–433.
[146] X.Y. Liu, W.J. Padilla, Adv. Mater. 28 (2016) 871–875.
[147] C. Xu et al., Adv. Mater. 32 (2020) 1905717.
[148] J. Guo et al., Appl. Surf. Sci. 402 (2017) 92–98.
[149] X.Y. Duan et al., Nat. Commun. 8 (2017) 14606.
[150] L. Phan et al., Adv. Mater. 25 (2013) 5621–5625.
[151] D.G. Baranov et al., Nat. Mater. 18 (2019) 920–930.
[152] M. Li et al., Sci. Adv. 6 (2020) eaba3494..
[153] E. Takasuka et al., J. Appl. Phys. 81 (1997) 6384–6389.
[154] J. Syurik et al., Adv. Funct. Mater. 28 (2018) 1706901.
[155] J. Mandal et al., Science 362 (2018) 315–318.
[156] P.C. Hsu et al., Science 353 (2016) 1019–1023.
[157] D. Urge-Vorsatz et al., Renew. Sustainable Energy Rev. 41 (2015) 85–98.
[158] P. Chandrasekhar et al., J. Appl. Polym. Sci. 131 (2014) 40850.
[159] A. Rougier et al., Ionics 14 (2008) 99–105.
[160] J.K. Tong et al., ACS Photonics 2 (2015) 769–778.
[161] R.J. Thorn, O.C. Simpson, J. Appl. Phys. 24 (1953) 633–639.
[162] Z. Yang, S. Ramanathan, IEEE Photonics J. 7 (2015) 0700305.
[163] W. Welnic, M. Wuttig, Mater. Today 11 (2008) 20–27.
[164] M. Wuttig, N. Yamada, Nat. Mater. 6 (2007) 824–832.
[165] M. Wuttig, S. Raoux, Z. Anorg. Allg. Chem. 638 (2012) 2455–2465.
[166] W. Yang et al., Acta. Phys. Sin-Chem. Ed. 63 (2014) 107104.
[167] E.E. Chain, Appl. Optics 30 (1991) 2782–2787.
[168] L. Mai et al., J. Phys. Chem. C 112 (2008) 423–429.
[169] M. Wei et al., Mater. Lett. 236 (2019) 350–353.
[170] K. Liu et al., Mater. Today 21 (2018) 875–896.
[171] Y. Qu et al., Light-Sci. Appl. 7 (2018) 26.
[172] J. Jian et al., ACS Appl. Mater. Interfaces 9 (2017) 5319–5327.
[173] M.A. Kats et al., Phys. Rev. X 3 (2013) 041004.
[174] Y. Ke et al., Adv. Energy Mater. 9 (2019) 1902066.
[175] Y. Ke et al., Small 14 (2018) 1802025.
[176] J.A. Beardslee et al., Chem. Vapor Depos. 16 (2010) 206.
[177] C. Adessi et al., J. Phys. Chem. Solids 138 (2020) 109180.
[178] C.-T. Wang, M.-T. Chen, Mater. Lett. 63 (2009) 389–390.
[179] C.-T. Wang, M.-T. Chen, Sensor Actuat. B-Chem. 150 (2010) 360–366.
[180] G.A. Niklasson, C.G. Granqvist, J. Mater. Chem. 17 (2007) 127–156.
[181] Y.G. Jeong et al., Adv. Opt. Mater. 8 (2020) 1900548.
[182] F.H. Chen et al., ACS Appl. Mater. Interfaces 7 (2015) 6875–6881.
[183] J. Bian et al., J. Mater. Sci. 51 (2016) 6149–6155.
[184] J.L. Andrews et al., Chem. Mater. 29 (2017) 3285–3294.
[185] Y. Xiao et al., Appl. Phys. Lett. 107 (2015) 031906.
[186] H. Ji et al., Sol. Energy Mater. Sol. C 176 (2018) 1–8.
[187] K. Tang et al., Adv. Mater. 32 (2020) 1907071.
[188] Y. Qu et al., Laser Photonics Rev. 11 (2017) 1700091.
[189] O.Y. Hao et al., Nanophotonics 9 (2020) 2351–2359.
[190] K. Du et al., Nanoscale 10 (2018) 4415–4420.
[191] Y. Qu et al., Opt. Express 26 (2018) 4279–4287.
[192] Y.R. Qu et al., Light-Sci. Appl. 7 (2018) 10.
[193] G. Catalan, Phase Transit. 81 (2008) 729–749.
[194] J. Ruppen et al., Phys. Rev. B 96 (2017) 045120.
[195] A. Shahsafi et al., Proc. Natl. Acad. Sci. USA 116 (2019) 26402.
[196] L. Phan et al., Chem. Mater. 28 (2016) 6804–6816.
[197] Y. Dong et al., ACS Nano 13 (2019) 9918–9926.
[198] G. Wang et al., ACS Nano 10 (2016) 1788–1794.
[199] L. Donaldson, Mater. Today 21 (2018) 6–7.
[200] J. Wang et al., Nanoscale Res. Lett. 13 (2018) 361.
[201] P. Zhao et al., Opt. Mater. 94 (2019) 378–386.
[202] J.H. Pikul et al., Science 358 (2017) 210–214.
[203] L. Zhang et al., J. Mater. Chem. C 3 (2015) 4883–4889.
[204] D.L. Henann et al., J. Mech. Phys. Solids 61 (2013) 2047–2066.
[205] T. Chen et al., Mater. Design. 90 (2016) 1069–1076.

[206] T. Chen et al., Polym. Test. 47 (2015) 4–11.
[207] L. Phan et al., ACS Appl. Mater. Interfaces 8 (2016) 278–284.
[208] R. Kautz et al., Adv. Mater. 30 (2018) 1704917.
[209] C. Xu et al., Adv. Mater. 32 (2020) 1905717.
[210] A. Chatterjee et al., Bioinspir. Biomim. 13 (2018) 045001.
[211] L. Phan et al., J. Mater. Chem. C 3 (2015) 6493–6498.
[212] E.M. Leung et al., Nat. Commun. 10 (2019) 1947.
[213] C.Y. Xu et al., Science 359 (2018) 1495–1500.
[214] Y. Cui et al., Adv. Mater. 30 (2018) 1706807.
[215] Y. Zhai et al., Science 355 (2017) 1062–1066.
[216] H. Bao et al., Sol. Energy Mater. Sol. C 168 (2017) 78–84.
[217] L.L. Cai et al., Adv. Mater. 30 (2018) 1802152.
[218] P.B. Catrysse et al., ACS Photonics 3 (2016) 2420–2426.